Determination of internal friction angle of rock materials using the drilling data

by

Iman Rostam sowlat

A thesis
presented to the University of Waterloo
in fulfillment of the
thesis requirement for the degree of
Master of Applied Science
in
Mechanical and Mechatronics Engineering

Waterloo, Ontario, Canada, 2022

© Iman Rostam sowlat 2022

Author's Declaration

I hereby declare that I am the sole author of this thesis. This is a true copy of the thesis, including any required final revisions, as accepted by my examiners.

I understand that my thesis may be made electronically available to the public.

Abstract

Rock cutting is a critical process occurring in several rock excavation activities such as drilling, cutting, sawing, and is common across various industries such as petroleum, geothermal, geo-technical, and underground engineering. Rock cutting or scratching test can be defined by the action of a cutting tool whose relative movement is parallel across to the surface of a material to be cut.

The current work is prepared with the objective of providing experimental evidence that the internal friction angle of rocks can be assessed using a scratch test with a blunt polycrystalline diamond compact (PDC) cutter. For this purpose, a comprehensive set of cutting experiments was carried out to determine the wear flat-rock friction coefficient in two limestones and one coarse-grained sandstone using state-of-the-art scratch based rock cutting equipment. Additional triaxial compression (TC) experiments were conducted on specimens of these rock formations, and a Coulomb failure analysis was conducted to independently estimate the internal friction coefficient of each specimen. The experimental results indicate that the value of internal friction angle (intrinsic rock property) derived from TC experiments is related to the apparent friction angle at the wear flat-rock interface of the blunt PDC cutter when the wear flat surface is inclined at inclination angles ranging between 0° to 1°. Further, new results on one rock specimen were obtained by performing novel scratch tests with blunt PDC cutters with different wear flat properties, showing that the apparent friction angle at the wear flat-rock interface of a blunt cutting tool is significantly affected by the wear flat roughness and the wear flat material properties.

Acknowledgements

The process of preparing this dissertation could not have been accomplished without the ongoing support of many people. First, I would like to sincerely thank my supervisor, Professor Hyock-Ju Kwon from the University of Waterloo for his contribution, guidance and support throughout my study. His guidance helped me in all the time of research.

I owe my deepest gratitude to Professor Brian Evans from Curtin University (Australia), who made me believe in myself and guided me through the whole process of my study and dissertation writing. I am sure that this research would not have been completed without his mentorship, support, understanding, and encouragement. He is the funniest advisor and one of the smartest people I know. I could not have imagined having a better advisor and mentor for my M.Sc. study.

I would like to express my sincere appreciation to Dr. Joel Sarout from CSIRO (Australia) and Professor Jamal Rostami from Colorado School of Mines (USA) for their constant guidance and encouragements, without which this work would not have been possible. For their unwavering support, I am truly grateful.

Dedication

To the soul of my mother for her endless love and prayers.

Table of Contents

List of Tables viii

List of Figures ix

1 Introduction 1

1.1 Introduction 1
1.2 Research objective and methodology 4
1.3 Organization of thesis 4

2 Literature Review 6

2.1 Mechanics of rock cutting 7
2.2 Sharp cutter 11
2.3 Blunt (worn) cutter 15

3 Experimental Setup 26

3.1 Scratching device 26
3.2 Testing Procedure 28
3.3 Cutters 29
3.4 Rock specimens and properties 34

4 Results and Discussion 42

4.1 Determination of internal friction angle 42
4.2 Effect of wear flat properties on apparent friction angle 50

5 Conclusion and Future Work 55

References 57

APPENDICES 68

A Drawings of the rock cutting machine 69

B Drawing of the cutter holder to change the inclination angle 70

List of Tables

3.1 Geometrical specifications of the cutters used for testing 34

3.2 Mechanical and physical properties of rock specimens used in this study . . 35

4.1 Comparison between the internal friction angle (φ) estimated from triaxial (TC) tests and the apparent friction angle (ϕ) of rock specimens obtained from scratch tests when $\beta = 0°$. 46

List of Figures

1.1 Schematic of an inclined PDC cutter and its friction angle 3

2.1 Schematics of ductile and brittle modes of failure 7

2.2 (a) Ductile mode of failure, and (b) typical force pattern in the ductile mode. Test conducted on Tuffeau limestone at d=0.45 mm 9

2.3 (a) Brittle mode of failure, and (b) typical force pattern in brittle mode. Test conducted on Tuffeau limestone at d=1.30 mm 9

2.4 Schematic of forces acting on a PDC cutter 10

2.5 Forces acting on a sharp PDC cutter 12

2.6 Plot of intrinsic specific energy (ε) versus uni-axial compressive strength (q) 13

2.7 Plot of scaled intrinsic specific energy ($\frac{\varepsilon}{q}$) versus different back rake angles 13

2.8 Flow of the cuttings with increase of back rake angle (θ) 15

2.9 Total force components acting on a PDC cutter 17

2.10 Forces acting on a blunt PDC cutter 18

2.11 Schematic of $E - S$ diagram 19

2.12 Schematic of boundary layer underneath a blunt cutter 21

2.13 Variation of friction angle with contact stress in phase I. Tests conducted on Vosges sandstone 22

2.14 Variations of stabilized contact stress in terms of friction coefficient of wear flat surface 23

2.15 Variations of friction coefficient in terms of roughness at the wear flat-rock interface 24

2.16 Effect of slider cleanliness 25

3.1 The rock cutting machine 27
3.2 Schematic of the new cutter holder with fine adjustable inclination angle . 28
3.3 Flattening the irregularities of rock specimen 29
3.4 Schematic of a PDC cutter against a carbide cutter 30
3.5 Conceptual measurement of irregularities of a rough surface 31
3.6 Optical profilometer 32
3.7 Wear flat roughness of (a) a rough blunt cutter, and (b) a polished blunt cutter 33
3.8 Dimensions of a rock specimen used for the scratch test 35
3.9 Functional representation of the Sanchez Technologies triaxial stress vessel available at Geomechanics and Geophysics Laboratory 38
3.10 Schematic representation of the Sanchez Technologies triaxial stress vessel . 39
3.11 Plot of shear stress versus effective normal stress. Tests conducted on Mountain Gold sandstone 40
3.12 Plot of shear stress versus effective normal stress. Tests conducted on Tuffeau limestone 41

4.1 Plot of (a) apparent friction coefficient (μ_{ES}) and, (b) apparent friction angle (ϕ) as a function of inclination angle (β). Tests conducted on Tuffeau limestone using blunt cutter *5B*. 43
4.2 Plot of (a) apparent friction coefficient (μ_{ES}) and, (b) apparent friction angle (ϕ) as a function of inclination angle (β). Tests conducted on Savonnieres limestone using blunt cutter *5B*. 44
4.3 Plot of (a) apparent friction coefficient (μ_{ES}) and, (b) apparent friction angle (ϕ) as a function of inclination angle (β). Tests conducted on Mountain Gold sandstone using blunt cutter *5B*. 45
4.4 Boundary layer of crushed rocks after scratch tests at two different depths of cut (d). Test conducted with a blunt PDC cutter on Mountain Gold sandstone 47
4.5 Scanning electron photo of the wear flat surface of the blunt cutter using Secondary Electron Microscope (SEM) 48

4.6 Material concentration plot in Counts Per Second (cps) versus Electron-Volt (ev) obtained by the SEM. Tests conducted on Savonnieres limestone . . . 49

4.7 Schematic of cuttings trapped on the wear flat surface in rock cutting at a constant depth of cut (d) . . . 50

4.8 Evolution of apparent friction coefficient (μ) and apparent friction angle (ϕ) versus wear flat roughness (R_a). Tests conducted on Tuffeau limestone when $\beta = 1.18°$ . . . 51

4.9 Evolution of friction coefficient (μ) and friction angle (ϕ) versus wear flat roughness (R_a). Tests conducted on Savonnieres limestone when $\beta = 9.70°$ 52

4.10 Plot of apparent friction coefficient as a function of inclination angle. Tests conducted on Tuffeau limestone with *carbide* cutter and PDC cutter *5B* . . 53

4.11 Plot of apparent friction coefficient as a function of inclination angle. Tests conducted on Savonnieres limestone with *carbide* cutter and PDC cutter *5B* 54

A.1 Schematics of rock scratching device. . . . 69

B.1 Drawing of the cutter holder used to change the inclination angle β (or the back rake angle θ). . . . 71

Chapter 1

Introduction

1.1 Introduction

Estimation of mechanical properties of rock materials is most often required in rock mechanics projects and in rock mechanics laboratory testing. The uni-axial compressive strength (q) and the internal friction angle (φ) are two key parameters needed to address a broad range of geomechanical problems found in civil, mining, and petroleum engineering, with applications ranging from the design of underground structures in rocks to the selection of tools for mechanical excavation [1–3]. In rock mechanics and rock engineering, various friction angles or coefficients have been discussed and used in practical applications including: (i) friction of the rock to rock surfaces on a joint, often measured by direct shear (DS) tests, (ii) internal friction angle of the rock that is often measured by triaxial compression (TC) tests, (iii) inter-granular friction of the grains when the rock is crushed, and (iv) friction between a tool and rock surface (apparent friction), among other concepts. These friction angles and related coefficients are inter-related and while they have different applications in the rock engineering world, they appear to have good correlations between different types of friction angles. If the correlations between these seemingly different friction coefficients are explored, in practice one might be able to use one to estimate the others that are unavailable or hard to measure. The focus of this research is to explore the possibility of replacing the expensive and time-consuming tests such as triaxial compression (TC) test with a simpler test such as scratch test to estimate the internal friction, specially where samples are scarce or limited.

A large number of methods have been developed over the years to estimate the uni-axial compression strength (q) [2, 4–9] while, the three main shear test approaches to estimate

the internal friction angle of rock are direct shear (DS), preset angle shear (PAS), and triaxial compression (TC) tests [10–18]. Among the above-mentioned methods, the "triaxial compression" test is one of the most trustworthy methods to obtain the internal friction angle of a specific rock specimen in which the cylindrical rock specimens are subjected to different values of uniform lateral confining pressures.

A triaxial compression (TC) test is a method for estimating the mechanical and strength properties of deformable solids such as rocks and soils, i.e. Young's modulus, Poisson's ratio, shear strength, cohesion, and internal friction angle. A typical TC test consists of: (i) subjecting a cylindrical rock specimen to the stress conditions at the stress levels of interest (usually a uniform confining pressure, and possibly a pore pressure); then (ii) superimposing an increasing axial stress at a constant confining pressure up to the failure of the rock. The recorded pre-failure deformation in the elastic regime allows for estimation of Young's modulus and Poisson's ratio for the given effective pressure in which the test was conducted. The failure attributes provide the estimation of the shear strength of the rock at given effective pressure. The data from multiple TC tests conducted at different effective pressures can be combined and analyzed in the mean-shear stress plane using the Coulomb failure criterion to determine the cohesion and the internal friction angle/coefficient of the rock specimen [19, 20]. The details of the TC test implemented in this study are provided in Section 3.4.

However, the TC test suffers from several drawbacks. One of the major drawbacks is that the TC test is relatively expensive and time-consuming [2, 3, 21–24]. In addition, the TC test requires high-quality and intact rock specimens, with adequate shape and size, i.e., cylindrical shape with a length to diameter ratio of two, and mutually-parallel end faces that must be orthogonal to the cylinder's axis. For instance, in the case of sedimentary rock specimens, it is difficult to core and extract the intact rock specimens from highly fractured and weak underground layers.

Previous studies [2, 7, 25–28] showed that the scratch test with a polycrystalline diamond compact (PDC) cutter is a promising approach for estimating the strength properties of rock specimens. The first advantage of the scratch test over a TC test is that specimen preparation is simple and no specific equipment or expertise is required to prepare the rock specimens. Secondly, the results of the scratch test are not affected by the dimensions of the rock specimen. Only a small piece of intact rock specimen is necessary to conduct the scratch test and estimate the internal friction angle. Thirdly, the test procedure is faster than a TC test because the necessary equipment is portable. Therefore, the test can be readily carried out on site (in the field). Finally, the tests can be repeated several times and each test lasts only a few minutes. However, similar to the TC test, the results of the scratch test also depend on the environmental conditions such as moisture

and temperature.

As shown in Fig. 1.1, during a scratch test with a blunt (worn) PDC cutter, the cutter shaves a layer of a rock specimen parallel to the sample's free surface [1] [19]. The friction induced on the wear flat by rock cuttings during the scratching process can be characterized by an "apparent friction coefficient" (i.e., cutter-rock friction). This coefficient is estimated from the normal and tangential force measurements and the orientation of the wear flat (see Section 2.3 for details). This apparent friction coefficient is in-principle different from the so-called internal friction coefficient of rocks, and quantifies the friction occurring between rock grains/particles that opposes shearing. The "internal friction angle" is derived from the slope of the linearised Coulomb failure envelope in the brittle regime. It is considered as an intrinsic property of the rock, i.e., different rocks have different internal friction coefficients.

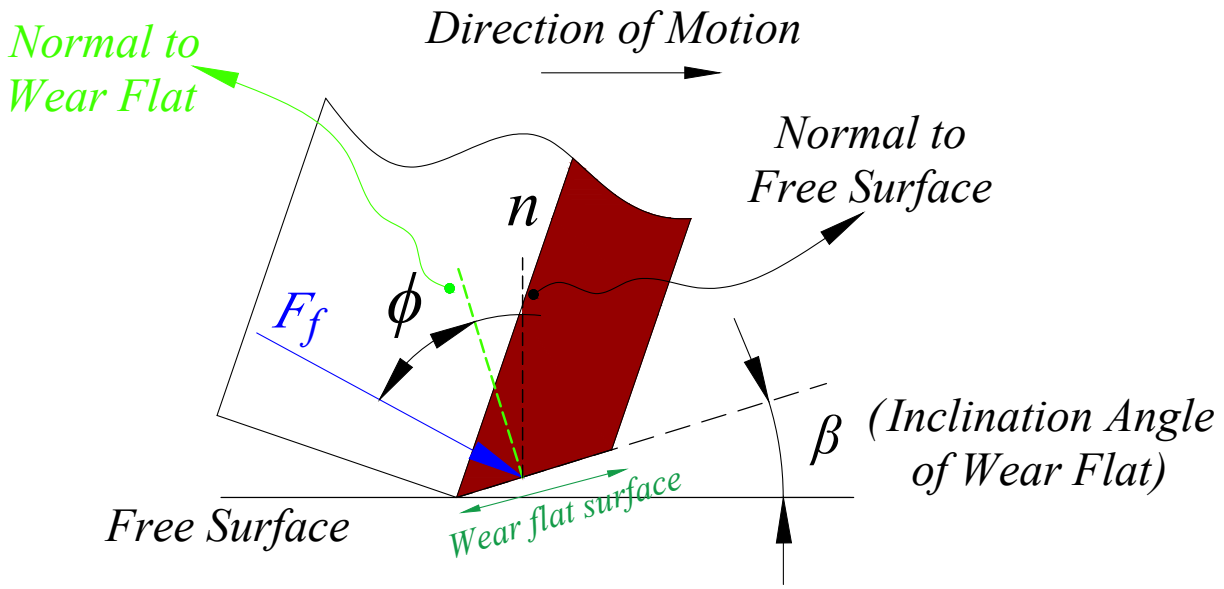


Figure 1.1: Schematic of an inclined PDC cutter and its friction angle.

[1] Free surface refers to the surface of the rock with no shear stress acting on it

1.2 Research objective and methodology

Nevertheless, to the best of my knowledge, no other reliable and robust investigation is devoted to the study of utilizing the scratch test to determine the internal friction angle (φ) of rocks with consideration of wear flat inclination angle (β). This research intends to determine the value of the apparent friction angle using scratch tests as well as finding a relationship between the apparent friction angle (obtained from the scratch test) with a blunt PDC cutter and the internal friction angle of the rock estimated from a TC test. In addition, the present research explores, for the first time, the effects of wear flat properties such as wear flat inclination angle, wear flat finish, and wear flat material on the determination of the internal friction angle of rock specimens. To this end, an extensive campaign of cutting experiments was performed on two limestones and one sandstone using various blunt polycrystalline diamond compact (PDC) and carbide cutters along with state-of-the-art rock cutting equipment. In parallel, I also used triaxial test equipment to measure the internal friction angles of the rock specimens under different values of lateral confining pressures.

1.3 Organization of thesis

The overall structure of the thesis takes the form of five chapters. Chapter 2 first provides a brief overview of the current state of the art in rock cutting with particular emphasis on the frictional process of blunt cutters. This chapter attempts to review the experimental and analytical studies relevant to the present investigation.

Chapter 3 is concerned with a detailed description of the laboratory equipment and testing procedure. I first describe the rock cutting or scratch machine, document the properties of the various cutters and rocks used for the study, and most important outline in details is the experimental procedures.

The fourth chapter presents the results of the cutting tests conducted on three quarry rock samples. This chapter focuses on the determination of the apparent friction angle at the wear flat-rock interface and its correlation with the internal friction angle of rock specimens. In addition, the influence of three main properties of the interface, namely the inclination angle, the wear flat roughness, and the wear flat material on the apparent friction coefficient as well as the apparent friction angle at the wear flat-rock interface is also investigated.

Chapter 5 draws final conclusions of this thesis, discusses the practical applications of the findings with a particular emphasis on using the scratch test as an alternative

approach to estimate the internal friction angle of rock materials. Further, this chapter outlines possible future avenues of research.

Chapter 2

Literature Review

Better understanding of the drilling data or rock cutting test to estimate the mechanical and physical properties of the rocks being drilling has been one of the main objectives of drilling research over the past decades and has continued in both theoretical and experimental areas. The oil field drilling operation has been mostly carried out using roller cone bits, which are indenters. Since being first introduced by General Electric (GE) in 1973 and put into use in the oil field in 1976, the PDC (Polycrystalline Diamond Compact) fixed-cutter bit or PDC bit has developed and progressed even since [29]. From then on, PDC bits were the substantial contributor in the economics of drilling industry for use in soft to medium-hard rock drilling due to their higher efficiency [30–35]. The emergence of new materials, in particular PDC (most often used on drill bits) in mid 70's, has led to a significant improvement in the drilling performance, that can be measured as the volume of rock excavated per cutting tool before the energy or power required to maintain acceptable productivity exceed the rig capabilities [36].

In the overwhelming majority of research studies, a single cutter is used to interact with the rock instead of a full-face bit. While full-scale experimentation provides a good imitation of the drilling operation, it is very expensive and time consuming. The response of a full-face bit can be modeled as the sum of the contributions of all the individual cutters distributed along distinct blades. Therefore, single cutter experiment is preferred as it is a relatively inexpensive experiment to model the bit-rock interaction mechanism [32, 36–39].

2.1 Mechanics of rock cutting

Rock cutting or rock scratching can be described as the shaving by machining of a layer of rock from a free surface using a tool moving parallel to the free surface. Better understanding of rock cutting or fragmenting has been one of the main objectives of drilling research since the 1950s and has continued up to now in both theoretical and experimental areas [40]. The PDC cutting tools cut and remove the rock surface and, therefore, the rock failure is taken place by a shearing process [41], which in turn, results in a faster drilling operation than roller cone bits [33, 42]. Furthermore, shearing rocks required less energy input to the system than crushing, since there is less energy wasted on the plastic deformation that occurs when crushing the rock. In the mid-1980s, over one third of the total footage drilled worldwide was done by PDC bits and from then on, PDC bits were developed with many technological advances which results in a growing share of drilling bit market [35, 36, 43].

Depending on the depth of cut (d) and the type of rock being cut, the rock failure mechanism involved in the cutting process is predominantly attributed to: (i) a ductile regime, and (ii) a brittle regime, see Fig. 2.1.

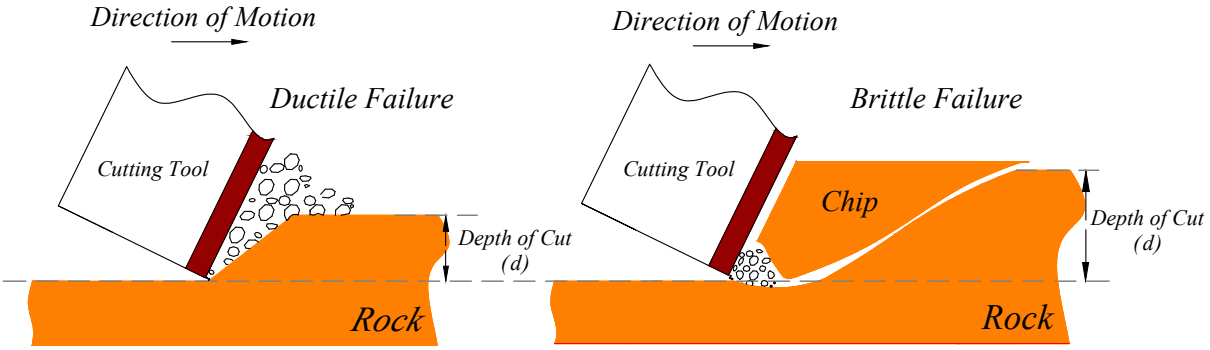


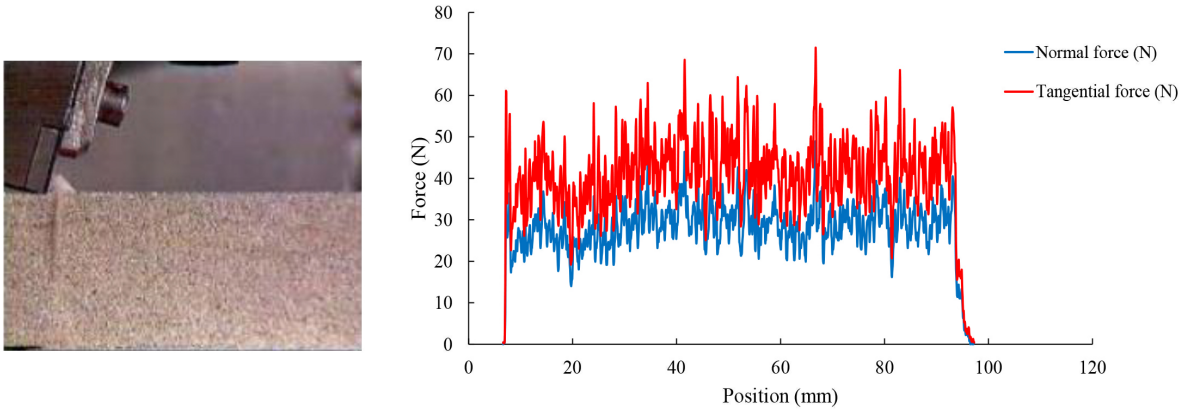
Figure 2.1: Schematics of ductile and brittle modes of failure.

The ductile regime (mode) is dominant at small cutting depths (typically less than 1 mm under atmospheric and dry conditions) and is characterized as a flow of cuttings or grains being sheared in front of the cutter and crushed at the tip of the cutter, as shown in Fig. 2.1 and Fig. 2.2a. As shown in Fig. 2.2b, the force signals resemble a white noise with a small spread between peaks within the ductile mode of failure. Once the cutting

face of cutter contacts the rock, the magnitudes of force components increase rapidly then reach relatively stable magnitudes throughout the scratch test [2, 44–47].

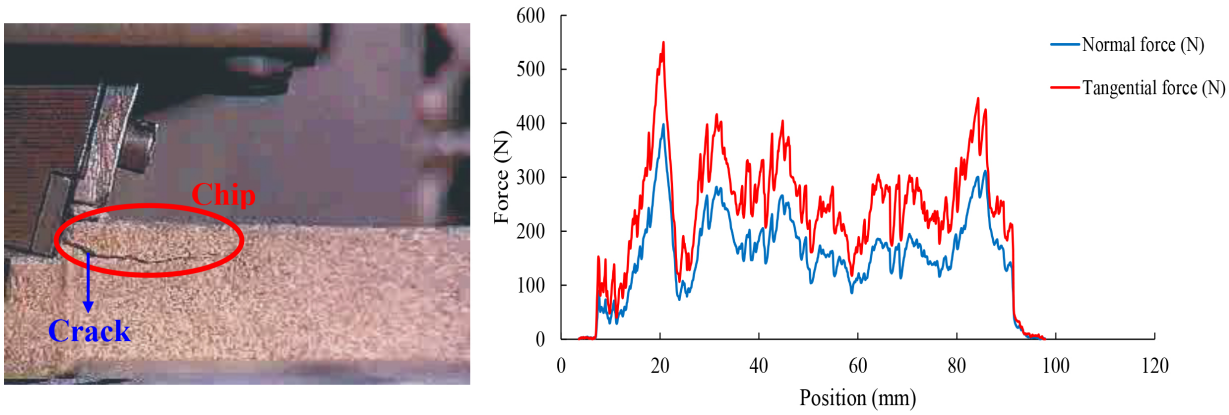
As shown in Fig. 2.1 and Fig. 2.3a, the brittle regime (mode) is characterized by incipient events; macroscopic cracks are initiated from the cutter tip and propagate between the grain boundaries, and eventually reach the free surface where a chip is formed and separates from the rock at large cutting depths, typically larger than 1 mm under atmospheric and dry conditions. When the chips are removed from the rock, the effective cutting depth drops to zero and increases until a new chip is reformed. Force signals depict a relatively larger spread between peaks and sudden drop in the force magnitudes after each peak due to chip formations, see Fig. 2.3b [44, 45, 48–50]. In contrast to the ductile regime, the average cutting force within the brittle regime of failure does not vary linearly with the depth (d) [2, 44, 47, 51–53].

Experimental and numerical observations by some researchers [54–60] have indicated that the cutting force over the cutting process is controlled by the fracture toughness (K_{IC}) of the rock in the brittle regime and by the uni-axial compressive strength (q) of the rock in the ductile regime. Note that these two modes of failure (ductile and brittle) correspond to the minimum energy dissipation at different depths of cut (d). The two regimes are interpreted by different theories, strength theory and LEFM (Linear Elastic Fracture Mechanics). When the cutting depth is small, the crushing mode dissipates less energy, and the force corresponding to strength theory is smaller than that corresponding to LEFM. On the other hand, the fracture mode dissipates less energy when the depth of cut is large, and the force corresponding to LEFM is smaller than that corresponding to strength theory. Therefore, the rock fails in a mode with minimum force. It is important to stress that all the scratch tests reported in this study were carried out in the ductile regime (depth of cut is smaller than 1 mm) of failure under atmospheric pressure and dry conditions.



(a) (b)

Figure 2.2: (a) Ductile mode of failure [44], and (b) typical force pattern in the ductile mode. Test conducted on Tuffeau limestone at d=0.45 mm [40].



(a) (b)

Figure 2.3: (a) Brittle mode of failure [44], and (b) typical force pattern in brittle mode. Test conducted on Tuffeau limestone at d=1.30 mm [40].

It is well accepted in the literature [37, 61–65] that the cutting action of a single PDC cutter is divided into two simultaneous processes: (i) "pure cutting" of the rock ahead of

the cutter, and (*ii*) "frictional contact" mobilized along the wear flat interface (underneath the cutter). Thus, assuming that a single cutter is tracing a groove with a constant depth of cut (d) and under constant horizontal velocity ($\boldsymbol{v}$), as shown in Fig. 2.4, the total force ($\mathbf{F}$) acting on such a cutter is the sum of the cutting force ($\mathbf{F_c}$) acting on the cutting face, and the frictional force ($\mathbf{F_f}$) mobilized across the wear flat surface, as presented in Eq. 2.1.

$$\mathbf{F} = \mathbf{F_c} + \mathbf{F_f} \tag{2.1}$$

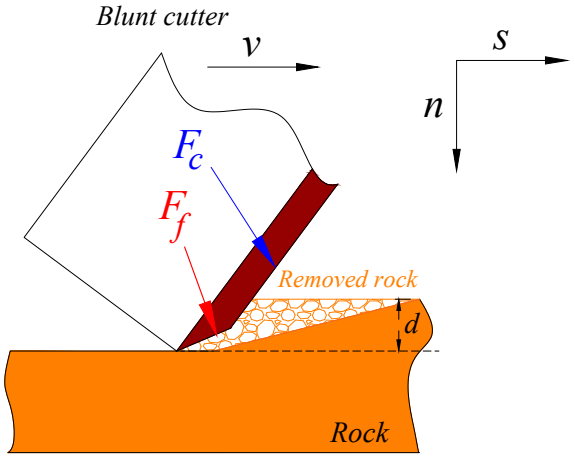


Figure 2.4: Schematic of forces acting on a PDC cutter.

The PDC cutting tools are classified into two main types: sharp cutter and blunt cutter. In the case of a sharp cutter, only one contact surface, the cutting face, is in contact with the rock specimen while for the blunt cutters, in addition to the cutting face, the wear flat surface interacts with the rock. The presence of the wear flat is the only indicator to differentiate a blunt cutter from a sharp cutter. The wear flat surface of the blunt PDC cutters is not the result of intensive cutting but is created by machining (grinding) sharp cutters [2, 40].

2.2 Sharp cutter

Consider first a sharp cutter of width ω that is moved steadily across a flat rock surface at a constant depth of cut (d) and with a back rake angle [1] of θ (positive when inclined forward). For such a cutter, the only force acting on the rock specimen is transmitted by the cutting face of the tool. Let this force be denoted as $\mathbf{F_c}$, and $\mathbf{F_{cn}}$ and $\mathbf{F_{cs}}$ are the force components in the direction normal (subscript n) and parallel (subscript s) to the cutter motion, respectively (see Fig. 2.5). Motivated by the self-similarity, Detournay & Defourny [37] assumed that cutting forces in both directions (averaged over a large distance -across the length of the rock specimen compared to the depth of cut to minimize the effect of any possible heterogeneities) are proportional to the cross-section area ($A_c = \omega \times d$, see Fig. 2.5):

$$\begin{cases} F_{cn} = \zeta \varepsilon A_c \\ F_{cs} = \varepsilon A_c \end{cases} \tag{2.2}$$

where the ratio ζ is given by:

$$\zeta = \tan(\theta + \psi) \tag{2.3}$$

and ψ is the inclination angle of the total cutting force ($\mathbf{F_c}$) to the normal of the cutting face (k) and ε is the intrinsic specific energy (as the work done to remove a unit volume of the rock using an ideally sharp bit/cutter in the pure cutting mode with the unit of MPa [37, 66]). Previous laboratory studies [2, 7, 25–27, 67] and numerical simulation [49] found that the scratch test with a single sharp PDC cutter can be considered as a promising approach to find the rock strength. A new experimental cutting test with double circular cutters [68] implied that when the distance between two circular PDC cutters is reduced, the specific energy decreases by 5% to 25% at large cutting depths. Hence, the concept of the intrinsic specific energy (ε) along with the mechanical (actual) specific energy (E) being put into the system can be the best approach to measure the drilling efficiency.

Laboratory experiments with single sharp PDC cutting tool under atmospheric pressure and dry environment indicated that the value of ε increases with increasing the back rake angle θ but is well correlated with the uni-axial compressive strength (q) of the rocks when $\omega \simeq 10 - 20$ mm and θ ranges from 10° to 20° in the case of rectangular cutting tool, see Fig. 2.6 [2, 7, 27, 69–73]. This range of the back rake angles is more commonly used for the cutters mounted on the distinct blades of PDC bits. However, Hareland *et al.* [74] believed

[1] The slant of the cutter, namely known as the back rake angle is defined as the angle between the velocity vector ($\boldsymbol{v}$) and the normal k to the cutting face face of the cutter, as shown in Fig. 2.5

that the back rake of 0° to 5° possesses the maximum drilling efficiency. More recently, in a comprehensive study investigating the effect of back rake angle [28], it was reported that the ε increases dramatically at very large back rake angles ($\theta > 75°$) while it is roughly half of the strength of rock materials (q) for negative rake angles ($\theta < 0°$) due to possibility of the brittle failure at negative back rake angles, see Fig. 2.7 [75]. Laboratory studies [76–78] suggested that an increase of cutting depth (d) and cutting speed ($\boldsymbol{v}$) leads to a decrease of ε. Experimental findings [73] also showed that ε under low confining pressure increases faster than high confining pressure.

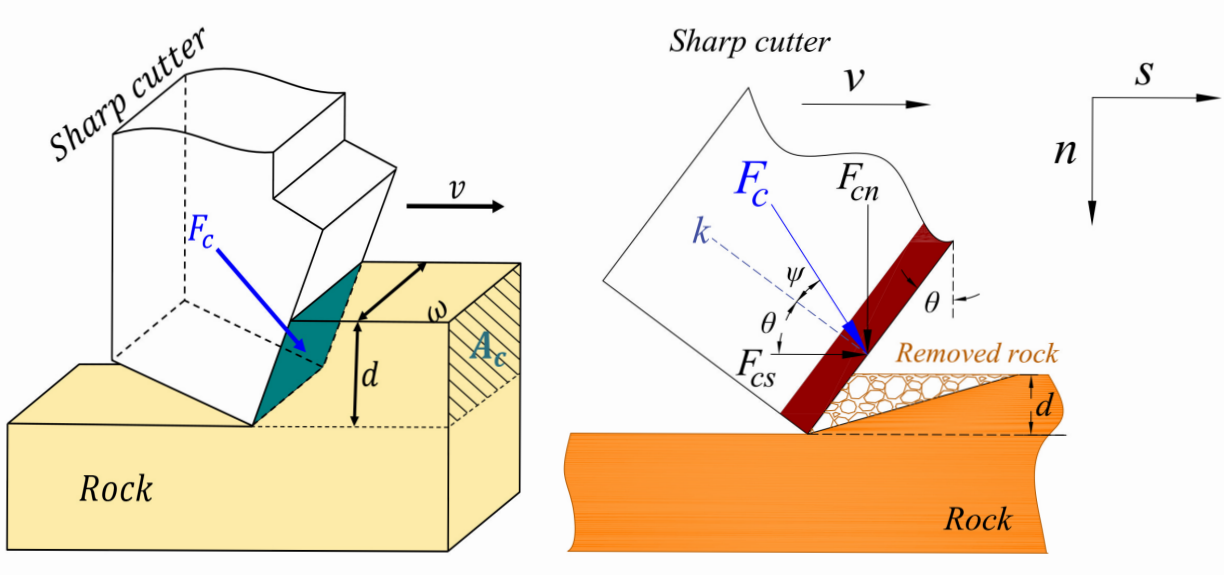


Figure 2.5: Forces acting on a sharp PDC cutter.

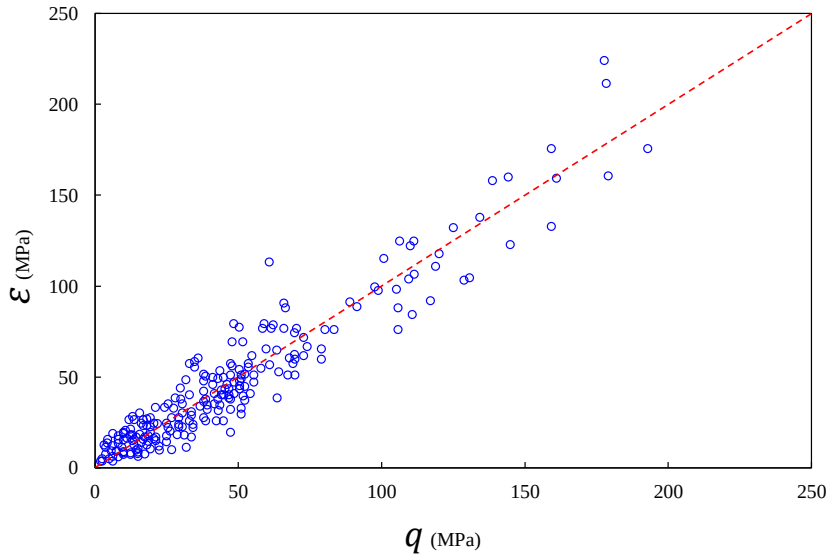


Figure 2.6: Plot of intrinsic specific energy (ε) versus uni-axial compressive strength (q) [2].

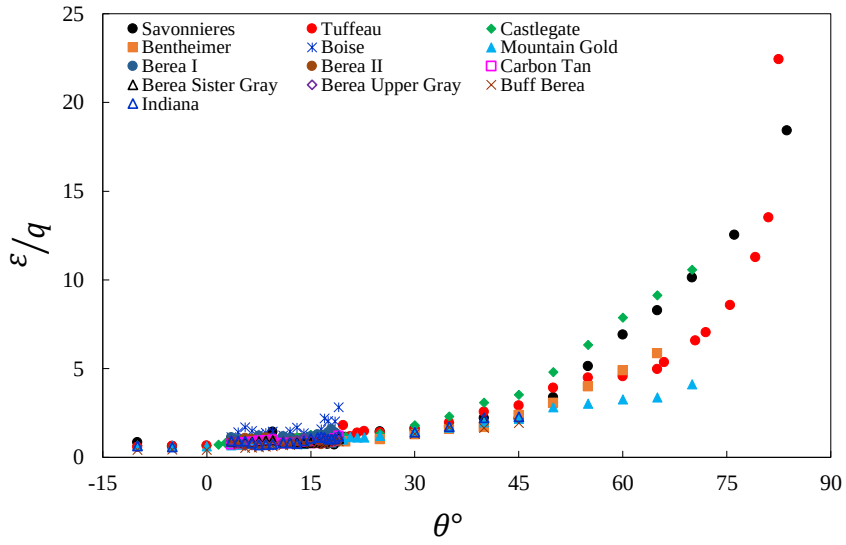


Figure 2.7: Plot of scaled intrinsic specific energy ($\frac{\varepsilon}{q}$) versus different back rake angles [28, 40].

The dimensionless number ζ characterizes the inclination of the total cutting force ($\mathbf{F_c}$), see Fig. 2.5. Thus, Wang *et al.* [79] proposed that the value of total cutting force (F_c) can be obtained by:

$$F_c = \frac{cA_c}{(b+1)\sin\chi\cos(\theta+\psi+\chi+\varphi)} \tag{2.4}$$

where c refers to the rock cohesion, φ refers to the internal friction angle of rock, θ refers to the back rake angle, ψ refers to the interfacial friction angle, χ refers to the shear failure angle, and b refers to the stress distribution coefficient that is given by:

$$b = 11.3 - 0.18\theta \tag{2.5}$$

On the other hand, it has been noticed that the number ζ is in the range of $0.50 \leq \zeta \leq 0.90$ for a back angle of 15° and in comparison with intrinsic specific energy, ζ appears to be relatively independent of the rock properties [41, 80, 81]. Equation 2.3 is generally based on the Amonton's second law of dry friction with consideration of a simple force balance on the cutting face of the cutter [82]. Experimental results [28, 72] suggested that ψ is independent of the d for a given θ. Numerical [49, 83, 84] and experimental [28, 72, 82, 85] studies reveal the dependency of the ψ on the θ which is caused by the existence of a flow process ahead of cutting face.

One possible interpretation [28, 44, 72, 75, 82] invokes the existence of a dead zone or build-up edge (BUE) of failed material forms at the bottom of the cutting face, which leads to a decomposition of the flow of cuttings into two directions including an upward flow and a backward flow. An increase of the back rake increases the backward flow at the expense of the upward flow responsible for variation of ψ, see Fig. 2.8. Results of cutting tests [28, 72] under atmospheric pressure and dry environment also indicated that the decrease of the ψ with increasing θ seems to follows a "universal trend" and slightly is a function of the rock type.

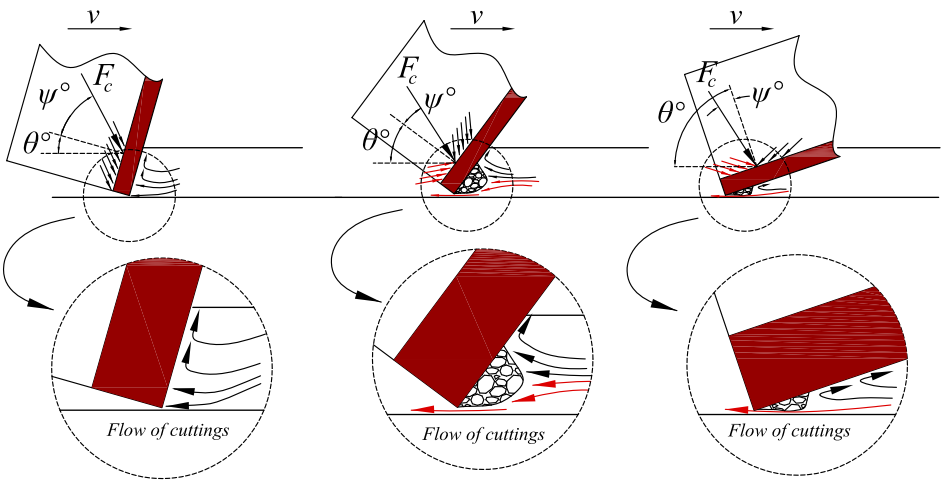


Figure 2.8: Flow of the cuttings with increase of back rake angle (θ) [28].

2.3 Blunt (worn) cutter

One of the main limitations of the different models proposed by researchers is that the influence of the wear face is often not considered in the model. Tests results with both sharp and blunt cutters were first presented by Glowka in the late 80s [63, 86]. The often-used model in drilling with PDC bits is Detournay & Defourny [37] (hereafter referred to as the "DD-model") originated from the suggestion of other researchers [61]. Accordingly, the DD-model indicates that the rock cutting is actually a combination of two independent operations: the "pure cutting" and the "frictional contact" on account of wear surface.

The DD-model was conformed with the findings of Glowka [63] and then developed to describe the rock cutting under ductile mode of failure (plastic deformation) which is most common for sedimentary rock samples. The DD-model was then supported experimentally by other researchers [41, 81, 87–89].

The DD-model is mainly constructed on the basis of three main assumptions:

1. the cutting process with a single PDC cutter can be modeled as two independent processes: "pure cutting" and "frictional contact",
2. the force acting on the cutting face is linearly related to the cut surface area (A_c), and

3. the force acting on the interface between the rock and the wear flat of a blunt PDC cutter is independent from the cutting depth and its normal and shear components are related by the friction law.

The existence of this wear flat surface leads to an additional force which is independent of the cutting force under assumption (1) and is assumed to take place at the interface between the rock and the wear surface, see Fig. 2.10. Similar to the cutting force, in the case of the blunt cutter with a wear surface with an inclination of β (see Fig. 2.10), it is assumed that there is an additional force, called frictional force ($\mathbf{F_f}$), acting on the wear flat surface, which is unrelated to the force $\mathbf{F_c}$. The frictional force ($\mathbf{F_f}$) vector can be decomposed into two components: $\tilde{F_{fs}}$ and $\tilde{F_{fn}}$, which are parallel and normal to the wear flat surface, respectively. These two frictional components are related by the friction law:

$$\tilde{F_{fs}} = \mu \tilde{F_{fn}} \tag{2.6}$$

where μ is the apparent friction coefficient at the wear flat-rock interface. As can be seen in Fig. 2.10, the terms $\tilde{F_{fn}}$ and $\tilde{F_{fs}}$ refer to the force components projected on the normal and tangent to the wear flat surface, respectively, which can be readily obtained through the following equation with consideration of the inclination angle (β) of the wear flat surface with respect to the direction of velocity vector ($\boldsymbol{v}$):

$$\begin{cases} \tilde{F_{fs}} = F_{fs} \ \cos\beta - F_{fn} \ \sin\beta \\ \tilde{F_{fn}} = F_{fn} \ \cos\beta + F_{fs} \ \sin\beta \end{cases} \tag{2.7}$$

Considering the Eq. 2.1, as depicted in Fig. 2.4 and Fig. 2.9, the tangential ($\mathbf{F_s}$) and normal ($\mathbf{F_n}$) components of the total force ($\mathbf{F}$) acting on a PDC cutter is given by:

$$\begin{cases} \mathbf{F_n} = \mathbf{F_{cn}} + \mathbf{F_{fn}} \\ \mathbf{F_s} = \mathbf{F_{cs}} + \mathbf{F_{fs}} \end{cases} \tag{2.8}$$

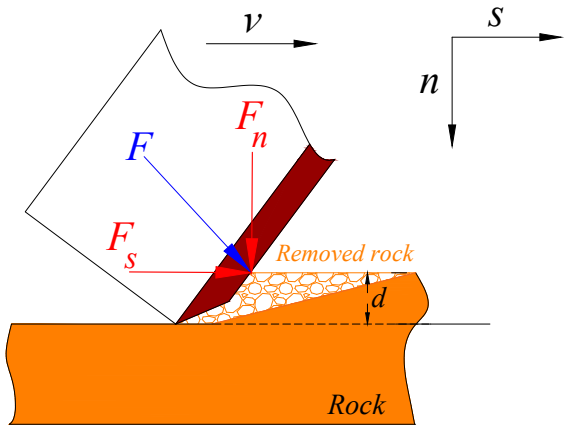


Figure 2.9: Total force components acting on a PDC cutter.

Therefore, the frictional force components separately can be obtained by the following equation:

$$\begin{cases} F_{fs}(d,\theta) = F_s(d,\theta) - F_{cs}(d,\theta) \\ F_{fn}(d,\theta) = F_n(d,\theta) - F_{cn}(d,\theta) \end{cases} \tag{2.9}$$

with $F_{cs}(d,\theta)$ and $F_{cn}(d,\theta)$ being, respectively, the force acting on a sharp cutter (the cutting face) in the tangential and normal directions to the cutter motion (see Fig. 2.5) for a given cutting depth (d) and back rake angle (θ), and F_{fs} and F_{fn} being, respectively, the total force acting on a blunt cutter (only the wear flat surface) in the tangential and normal directions to the cutter motion for a given cutting depth (d) and back rake angle (θ), as shown in Fig. 2.10. Put simply, to measure the forces only acting on the wear flat surface of a blunt PDC cutter at a certain depth of cut (d) and at a certain back rake angle (θ) in the laboratory rock scratch tests, we must first measure the total forces (normal and tangential) acting on the sharp PDC cutter. By subtracting these forces from the corresponding forces acting on the blunt PDC cutter at the similar depth of cut as well as the similar back rake angles, the acting forces on the wear flat surface of a blunt PDC cutter can be readily measured.

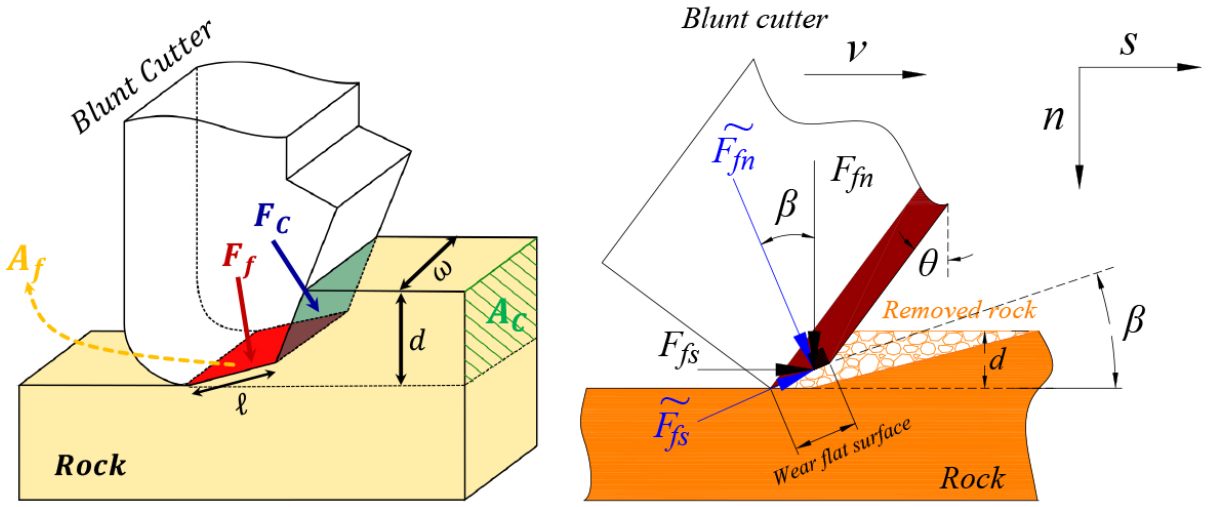


Figure 2.10: Forces acting on a blunt PDC cutter.

In light of Eqs. 2.2, 2.6, and 2.8, the tangential component of the total force acting on a single blunt cutter thus can be expressed as:

$$F_s = \varepsilon A_c + \mu F_{fn} \tag{2.10}$$

Replacing F_{fn} with $F_n - F_{cn}$ and applying Eq. 2.2, Eq. 2.10 becomes:

$$F_s = (1 - \zeta\mu)\varepsilon A_c + \mu F_n \tag{2.11}$$

For a blunt cutter, there exists a linear relationship when the cutting and frictional processes take place simultaneously, which is obtained by dividing both sides of Eq. 2.11 by A_c:

$$E = E_0 + \mu S \tag{2.12}$$

where E_0 is a constant defined as:

$$E_0 = (1 - \mu\zeta)\varepsilon \tag{2.13}$$

and,

$$\begin{cases} E = \frac{F_s}{A_c} \\ S = \frac{F_n}{A_c} \end{cases} \tag{2.14}$$

Equation 2.12 is represented graphically in a synthetic E-S diagram, see Fig. 2.11, by a line with a slope μ_{ES}, intercepting the E-axis at E_0. This line is defined as the friction line. All admissible states of the response of a blunt PDC bit lie on the friction line above and to the right of the cutting point. The cutting point is the point at the intersection of the friction line with the cutting locus, the line that goes through the origin with the slope of ζ^{-1}. Experimental observations showed that the cutting efficiency increases significantly at the cutting point [32, 37, 81, 88, 90] since the effect of wear flat surface is minimized (negligible) and the rock is mostly removed by the cutting face. Therefore, the cutter consumes less energy to cut the rock specimen.

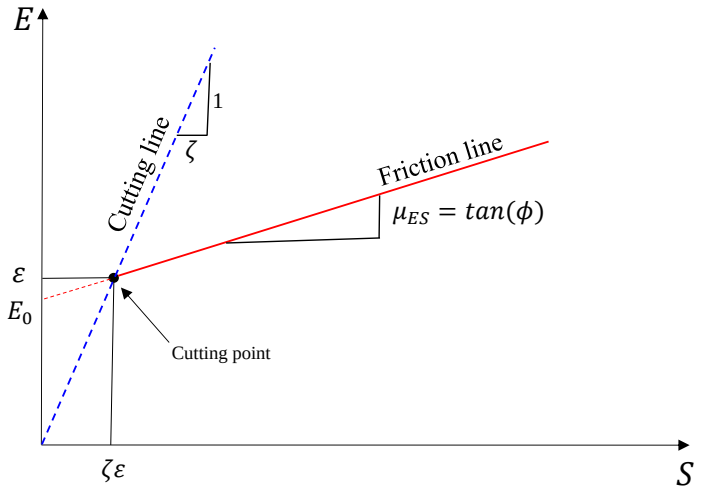


Figure 2.11: Schematic of $E - S$ diagram.

The apparent friction coefficient (μ_{ES}) is inferred from the slope of the best linear fit of the $E - S$ diagram of the cutting test conducted with a blunt PDC cutter which is found to be independent of the depth of cut [40, 91]. However, the magnitude of μ_{ES} is found to be a function of blade width in the case of a full scale bit [60]. As a consequence, with consideration of inclination angle (β), the apparent friction angle (ϕ) (the angle between the normal to the wear flat and the total frictional force acting on the wear flat, see Fig. 1.1) is obtained through the following equation [32, 37, 40, 88, 91–93]:

$$\phi = \arctan(\mu_{ES}) - \beta \tag{2.15}$$

The $E - S$ diagram obtained from scratch tests with blunt PDC cutters performed at Sandia National Laboratories [63], Imperial College London [41, 87, 90] and, the University of Minnesota [81, 88, 92] for different types of rocks and cutters provide strong support for the conjecture of Detournay & Defourny [37] and Samiselo [87] that the contact friction coefficient (apparent friction coefficient) at the wear flat-rock interface underneath the cutter is actually related to the property of the rock specimen being cut. Also, it has been observed that the apparent friction angle (ϕ) can be similar to the internal friction angle of the rock (φ) due to the existence of a boundary of failed cuttings, as shown schematically in Fig. 2.12. They concluded that the value of the apparent friction angle at the wear flat-rock interface is predominately controlled by the presence of a boundary layer of failed rocks (cuttings) underneath the cutter wear flat during the rock cutting with the blunt cutting tools.

The existence of a boundary layer of loose particles on the interface between a cutting tool and the rock surface is well supported by numerous experimental observations [52, 88, 90, 92–94]. Lhomme [92] studied the effect of the cutting tool cleanliness on the apparent friction coefficient. He carried out various tests on different rocks using blunt PDC cutters. He observed experimentally that the apparent friction coefficient of the contact surface of the cutting tool sliding on a rock surface significantly depends on the cutter history. The initially smooth surface of relatively soft materials like steel is influenced by the formation of ridges and grooves resulting from the action of harder asperities or wear cuttings. He carried out scratch tests by cleaning the wear flat surface of the PDC cutter after each scratch test. The findings indicated that wear flat cleaning significantly modifies the frictional properties, as presented in Fig. 2.16. Adachi [88] also carried out cutting tests on Red Wildmoor sandstone using a PDC blunt cutter. He found that the apparent friction angle (ϕ) at the wear flat-rock interface of the blunt PDC cutter is comparable to the internal friction angle of the rock specimen.

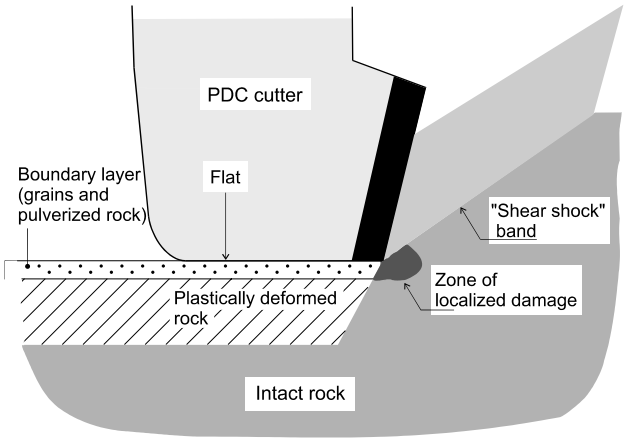


Figure 2.12: Schematic of boundary layer underneath a blunt cutter [88].

Lhomme [92] also carried out various tests under controlled normal force on various rocks using metallic and carbide sliders. Once the contact stress reaches the stabilized contact stress ($\sigma = \sigma_*$), the apparent friction coefficient levels off as well, see Fig. 2.13. Numerous studies [80, 88, 92, 93, 95] show that, in the second mode ($d_* \leq d \leq d_{**}$), the apparent friction angle (ϕ) mobilized at the wear flat-rock interface under specific conditions is remarkably close to the internal friction angle (φ), estimated from the conventional tri-axial compressive experiments deduced from the Mohr-Coulomb failure envelope.

A few researchers [92, 93] observed that for low values of the contact stress ($\sigma < \sigma_*$), the apparent friction coefficient of metallic tool sliding on a rock surface highly depends on the tool history. The initially smooth surface of relatively soft materials like steel is affected by the formation of ridges and grooves resulting from the action of the rock harder asperities or wear particles. Lhomme [92] conducted many tests by cleaning the surface of the cutting tool after each test and found that cleaning modifies dramatically the frictional properties.

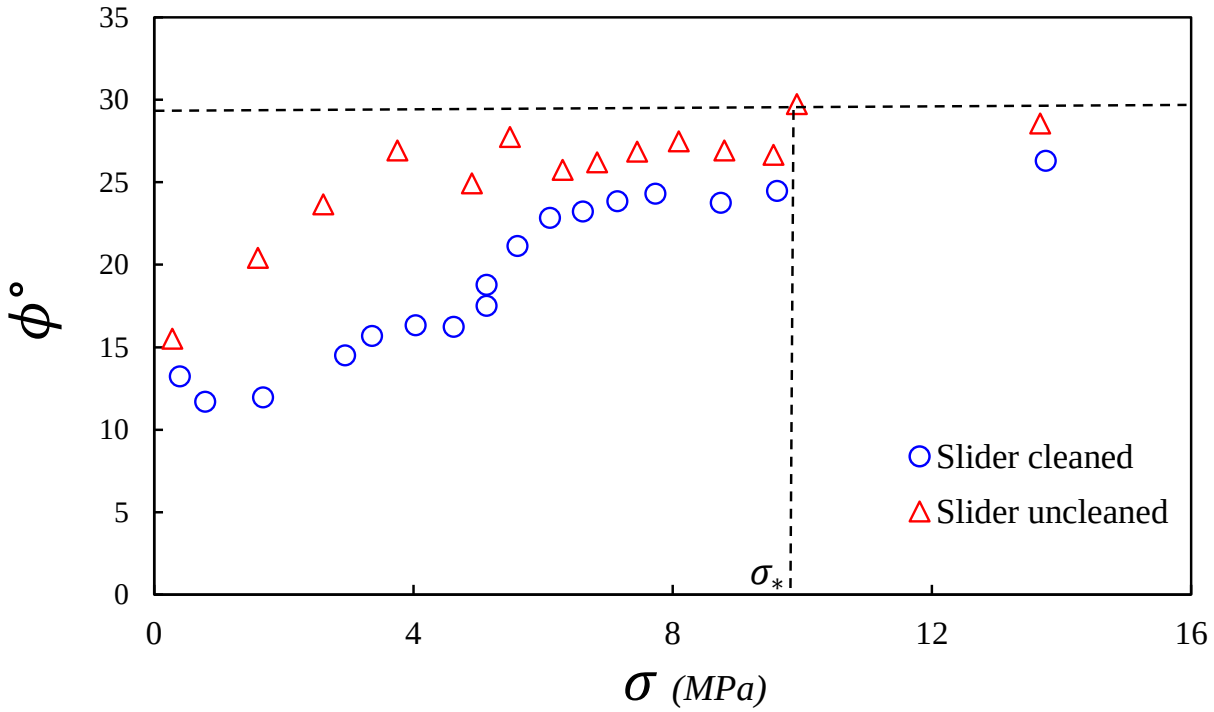


Figure 2.13: Variation of friction angle with contact stress in phase I. Tests conducted on Vosges sandstone [92].

Dagrain [93] performed comprehensive cutting tests under both controlled normal force and controlled cutting depth with both polished and rough blunt PDC cutters. The results showed that the limit stress (σ_*) decreases with increasing the apparent coefficient of friction (μ), where μ is itself affected by the properties of the wear flat surface such as roughness. As can be seen in Fig. 2.14 and Fig. 2.15, increasing the wear surface roughness (R_a) results in an increase of the limit apparent coefficient of friction (μ_*), which in turn leads to a decrease of the limit contact stress (σ_*). Further investigations [93, 96] implied that the wear flat area is not a parameter significantly influencing not only the contact stress but also the limit apparent coefficient of friction. More recently, experimental observations [91] argued that the limit apparent friction coefficient is not affected by the inclination angle of wear flat surface, however, the contact stress is influenced by variation of wear flat roughness under different inclination angles.

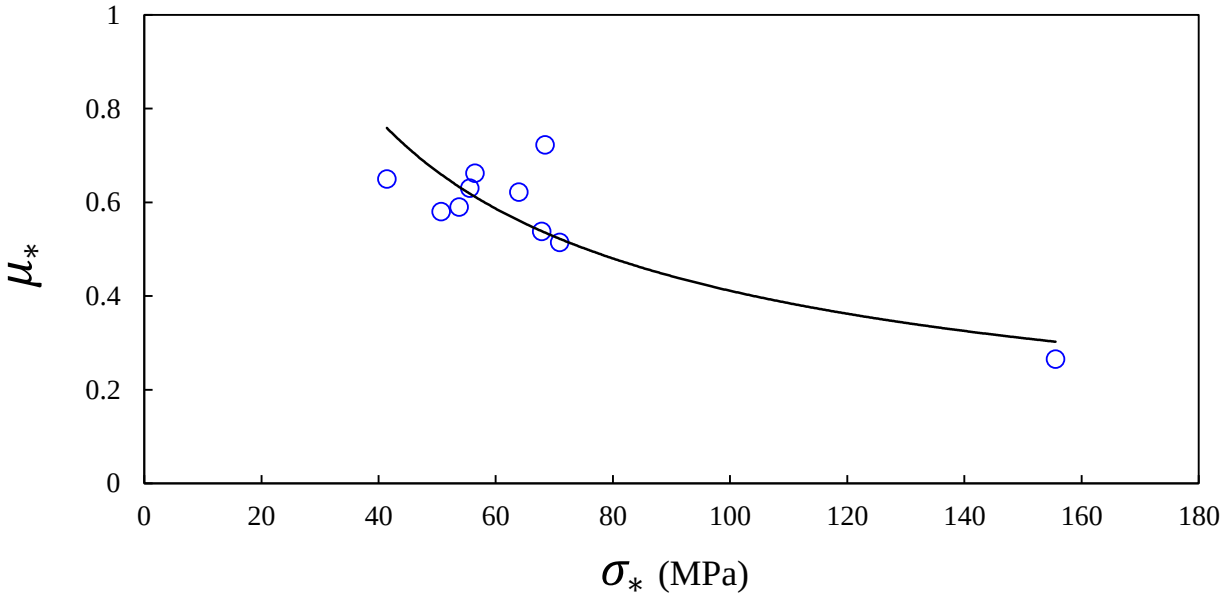


Figure 2.14: Variations of stabilized contact stress in terms of friction coefficient of wear flat surface [93].

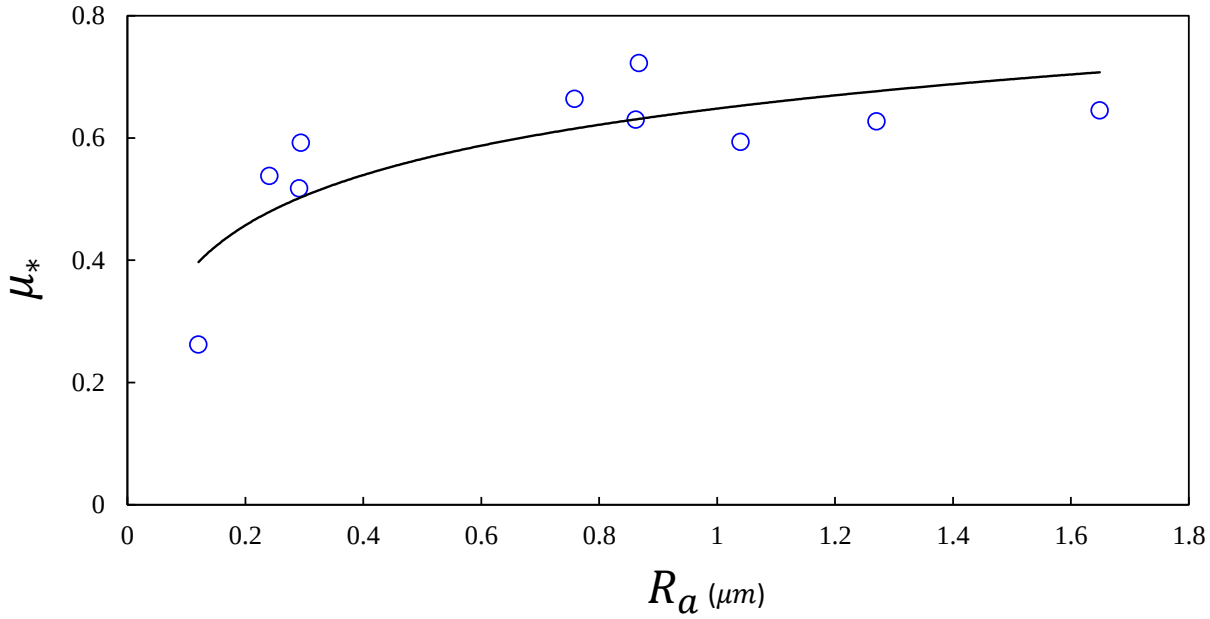


Figure 2.15: Variations of friction coefficient in terms of roughness at the wear flat-rock interface [93].

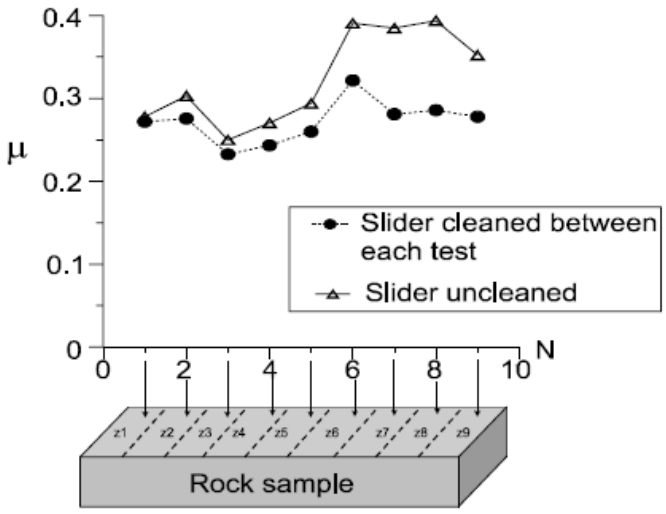


Figure 2.16: Effect of slider cleanliness [92].

The above literature provides experimental evidence suggesting the existence of a layer of loose rock particles at the tool-rock interface. Nevertheless, one of the main shortcomings of the previous studies is that the effect of inclination angle of the wear flat surface (β) on the apparent friction angle (ϕ) was not accounted for. Furthermore, to date, far too little attention has been paid to the influence of wear flat properties on the apparent friction angle.

Chapter 3

Experimental Setup

3.1 Scratching device

The experiments were carried out using a state-of-the-art scratch apparatus and housed at Geomechanics and Geophysics Laboratory (CSIRO), as schematically shown in Appendix A. The scratch machine performs semi-automated high precision scratching tests with a predetermined constant horizontal velocity ($\boldsymbol{v} = 4\ \frac{mm}{s}$) and constant depth of cut (d). The rock cutting experiment is carried out by cutting the rock specimen with a cutting tool, the PDC cutter, and making a groove of constant cross-sectional area at a certain cutting depth ($A_c = \omega \times d$, see Fig. 3.1c). As shown in Fig.3.1a, this apparatus consists basically of two perpendicular mechanical parts: (i) a horizontal bed where the rock specimen is held and tightened by a clamping system, and (ii) a Carriage Tower where the load cell, the cutter holder, and the cutter are situated, (see Fig.3.1b). The rock scratch device is equipped with an accurate load-cell to record the normal (n), tangential (s) and, lateral (t) components of the total force (Fig.3.1c) acting on the cutter separately along the entire rock specimen with a precision less than 1 N over a range of 0 to $\pm$3500 N.

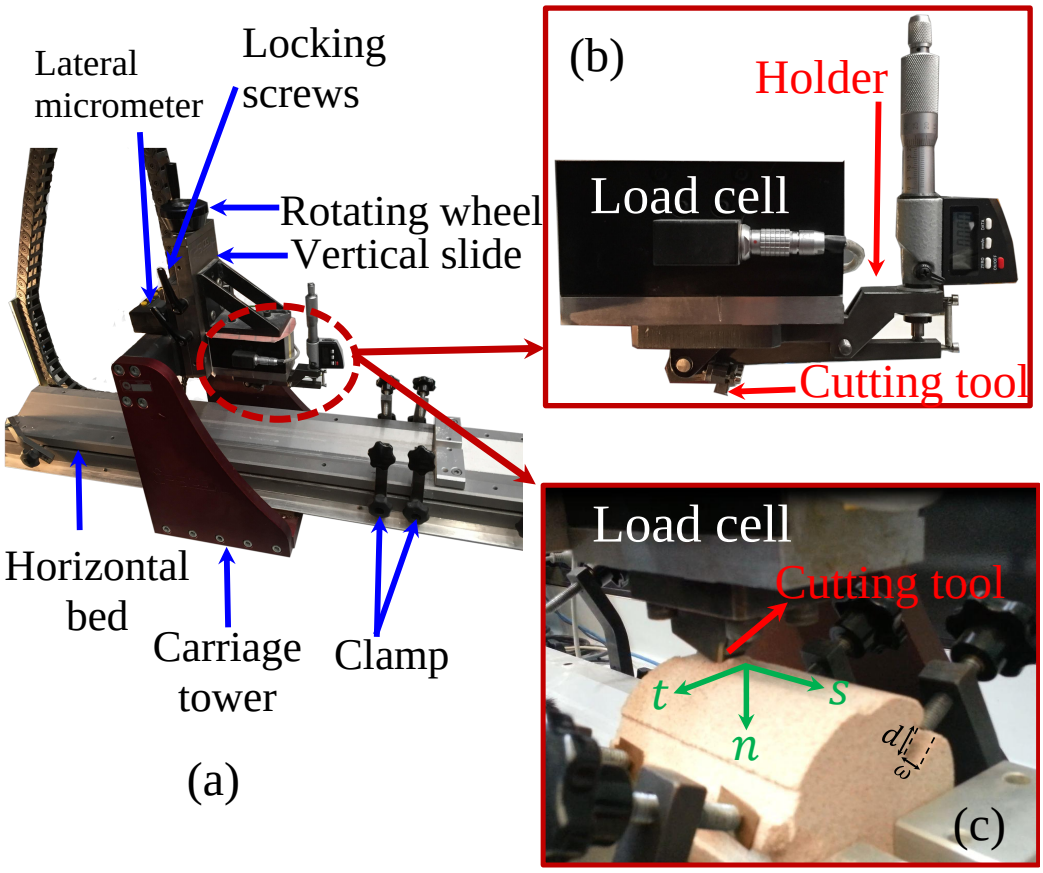


Figure 3.1: The rock cutting machine.

As shown schematically in Fig. 3.2, a novel cutting tool holder was designed (using AutoCAD 2015) and manufactured to vary the back rake angle (θ) as well as the inclination angle (β) of the wear flat surface of a blunt PDC cutting tool with the precision of 0.10° [39, 40, 91]. The main mechanical parts of the cutter holder are depicted in Fig. 3.2. In addition, the drawing of this cutter holder with the geometrical details is presented in Appendix B. The fixed body of the holder is attached to the base of the load cell. This cutter holder employs rotation of the adjustable arm around its center of rotation (center of the high tensile screw) in the range of 0° to 6.5°. To cover a broader range of inclination angles (β), extra cutter seats with different inclinations of the flat surface were designed and manufactured [39, 40, 91].

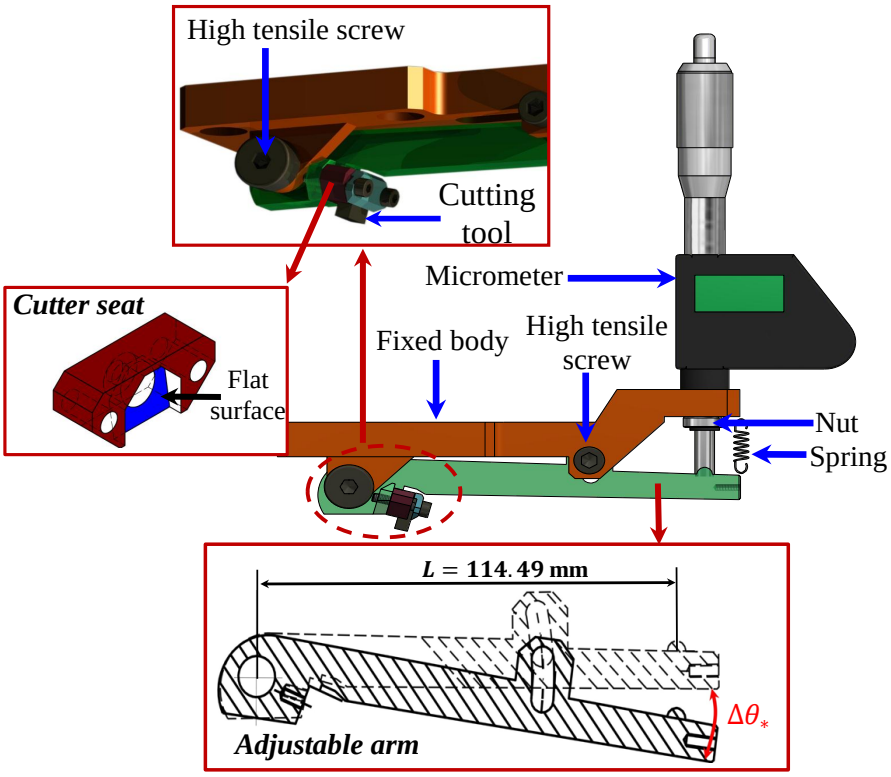


Figure 3.2: Schematic of the new cutter holder with fine adjustable inclination angle.

3.2 Testing Procedure

The rock specimen should be first checked visually to assess its level of inhomogeneity as well as existence of any macro-cracks. The rock specimen is then clamped firmly on the bed of the scratch device to avoid sliding or rotation of the specimen during the cutting test.

One or several primary cuts are required prior to any test series (Fig. 3.3a) to provide a flat grooved surface of width equal to the cutter width (Fig. 3.3b) over the length of test that is envisaged. The first depth of cut is roughly estimated by positioning the cutter tip at a given location below the highest point of the sample surface. Subsequent depths of cut are adjusted relative to the previous groove level. From one test to another, the depth of cut is adjusted relative to the prior groove. Practically, the micrometer is reset to zero

after the depth of cut has been adjusted and before the test is run. A cut can produce damage on the surface of the groove which can influence the next cut. Therefore, it is necessary to continuously check the groove surface and if necessary to perform at least one or a few levelling cuts at very shallow depths (typically around 0.15 mm).

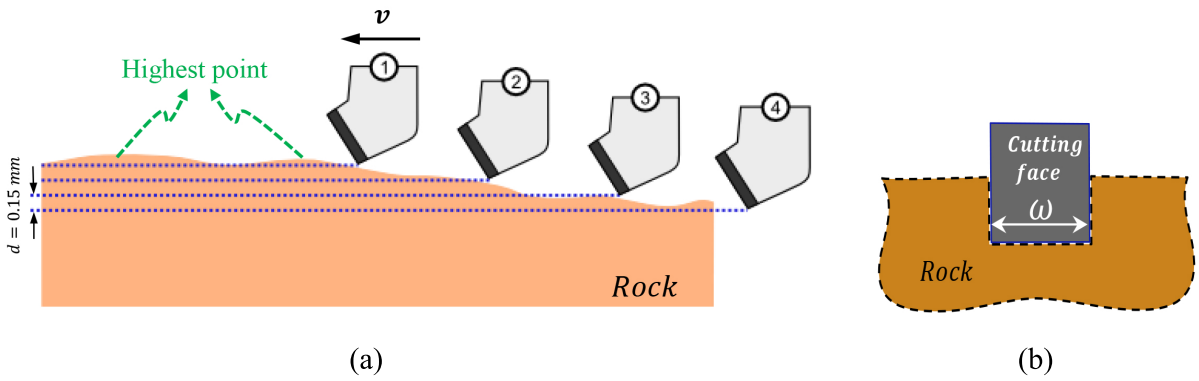


Figure 3.3: Flattening the irregularities of rock specimen.

From then onwards, successive cutting tests can be performed on the same groove at different depths of cut ranging from 0.10 mm to 0.90 mm in steps of 0.10 mm. After carrying out a test, both the rock and cutter surfaces are cleaned with a brush. Additionally, a vacuum cleaner can also be utilized to remove cuttings from the groove. Note that this testing procedure follows a standard method explained in several references [2, 28, 38–40, 44, 88].

3.3 Cutters

Five blunt PDC cutters (*5B*, *5D*, *M1*, *M2*, *M3*) and one blunt *carbide* cutter were used in this study. In general, the PDC cutters consist of an insert of PDC of rectangular shape, mounted on a piece of tungsten carbide [35]. The polycrystalline diamond compacts are produced by inserting diamond grits during a high pressure-high temperature (HPHT) process over 1400°C and 5.5 GPa using the belt press or cubic press technologies [36]. The thin layer of polycrystalline is atop a carbide substrate for the oil field drill bit applications [31, 35, 97–99]. It is important to note that the main difference between the PDC blunt cutter and the carbide blunt cutter is that both the wear flat surface and the cutting face

of the PDC blunt cutter are made of polycrystalline diamond compact while in the case of the carbide cutter, both the wear flat and the cutting face are made of carbide material, as schematically shown in Fig. 3.4. The width (ω) and thickness of all cutters are 10 mm and 5 mm, respectively. However, the roughness (R_a) of wear flat surfaces of the cutters vary from one cutter to another.

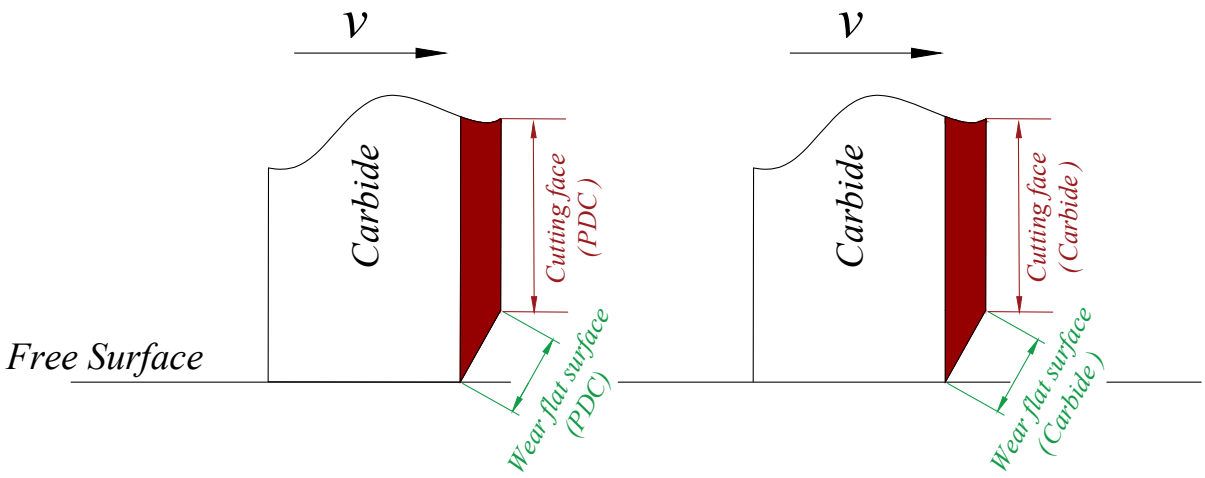


Figure 3.4: Schematic of a PDC cutter against a carbide cutter.

The average surface roughness (R_a) is the average distance between individual peaks and troughs (asperities) from the arithmetic mean[1] elevation of the profile (micro-irregularities), as conceptually shown in Fig. 3.5. Simply, R_a is the average of a set of distances between surface peaks and surface throughs. The average roughness is computed along the line of the sample using the following equation:

$$R_a = \frac{1}{n} \sum_{i=1}^{n} |z_i| \,. \tag{3.1}$$

[1]The mean line is located so the sum of areas above the line is equal to the sum of areas below the line.

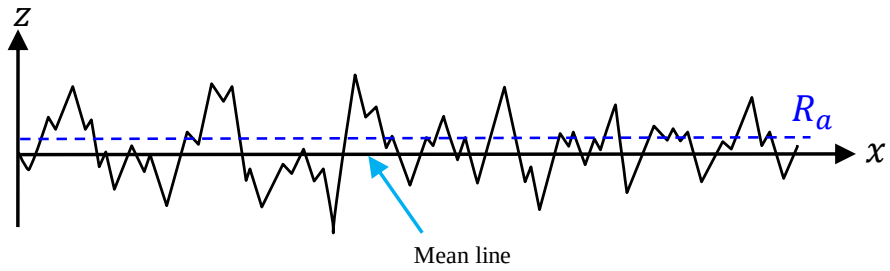


Figure 3.5: Conceptual measurement of irregularities of a rough surface.

I measured the wear flat roughness (R_a) with an optical profilometer WYKO NT1100 (located at the University of Waterloo), as depicted in Fig. 3.6. This optical profilometer is based on the light excitation and the depth detection using a beam positioned above the rock specimen. Fig. 3.7 reveals 3D photos of the roughness of the wear flat surface of a polished and a rough blunt PDC cutter obtained using the optical profilometer. It is obvious from Fig. 3.7 that due to visible high peaks on the wear flat surface of the rough cutter, the surface of the polished wear flat is much smoother than the rough cutter surface. In addition, we used a high resolution optical microscope (model AxioScope Imager A1) used with the ZEN software to measure the geometrical properties of the blunt cutters such as the wear flat length (ℓ) and the width (ω). The geometrical details of the blunt cutters are listed in Table 3.1.

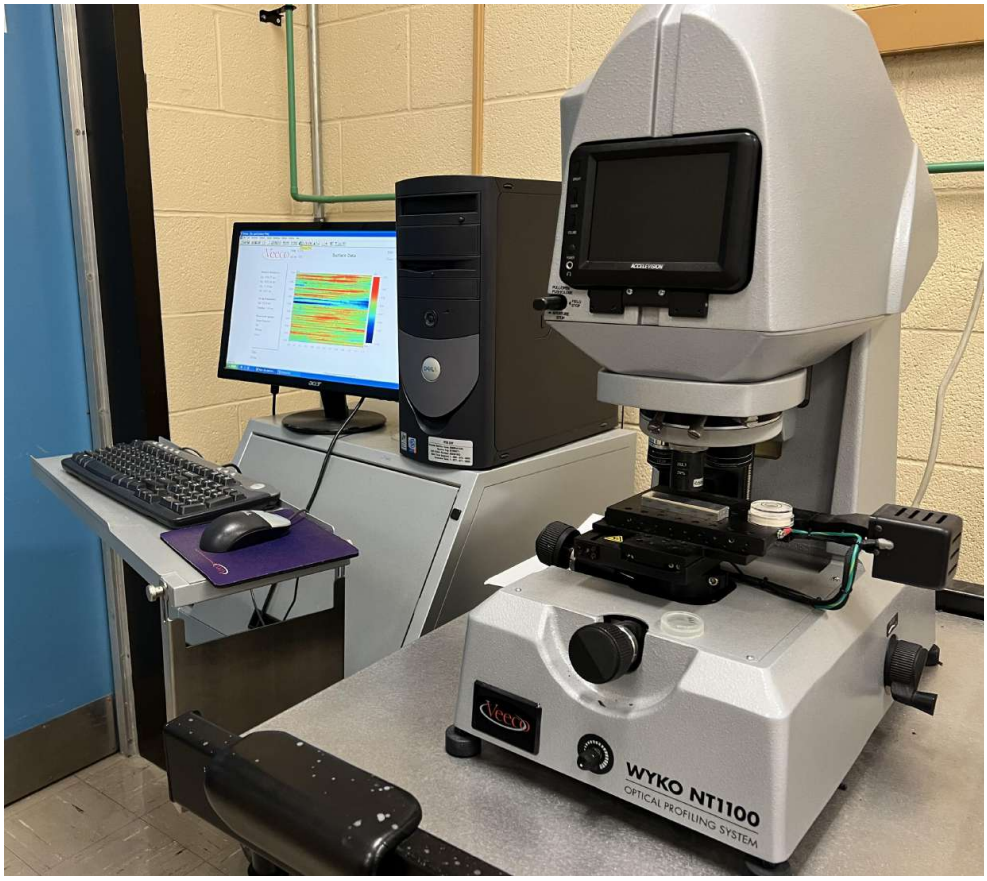


Figure 3.6: Optical profilometer.

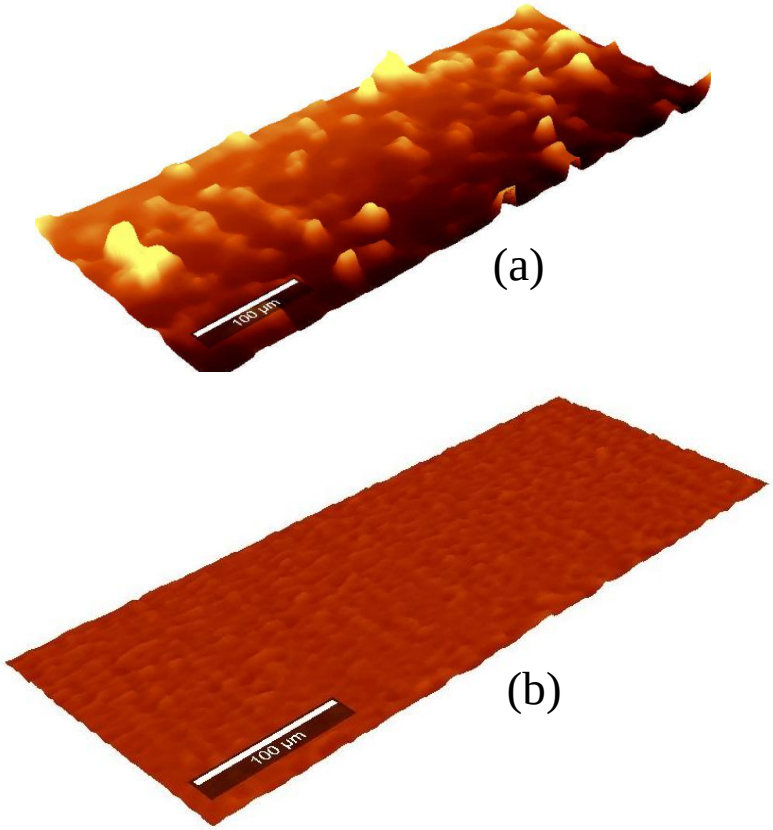


Figure 3.7: Wear flat roughness of (a) a rough blunt cutter, and (b) a polished blunt cutter.

Table 3.1: Geometrical specifications of the cutters used for testing [40].

Cutter	$\omega(mm)$	$\ell(mm)$	$A_f(mm^2)$	R_a (μm)
Blunt 5B	10	1	10	0.38
Blunt 5D	10	0.80	8	0.87
Blunt M1	10	1.51	15.11	0.65
Blunt M2	10	1.67	16.77	0.98
Blunt M3	10	0.76	7.66	1.42
Blunt Carbide	10	1.09	10.90	N/A

ω: Cutter width, ℓ: Wear flat length, A_f: Wear flat area, R_a: Wear flat roughness.

3.4 Rock specimens and properties

For the validation of the scratch testing approach, three rock specimens used in the experiments were the Mountain Gold sandstone, Tuffeau limestone, and Savonnieres limestone with no obvious damage on the rock's surfaces. Based on visual inspection, these rock specimens are reasonably homogeneous at the scale of the retrieved blocks. In this context, all specimens extracted from the same block have virtually identical properties (mineralogy, grain size distribution, elastic moduli, and mechanical strength). For each rock specimen, several cylindrical specimens (80 mm in diameter and 120 mm in length, see Fig. 3.8 and Fig. 3.1c) were cored from the same block for scratch testing. In order to further minimize the influence of rock heterogeneity, the scratch test was repeated three times on three different sides of each cylindrical specimen.

Table 3.2 lists the basic physical and mechanical properties of these three rock specimens as reported by Rostamsowlat *et al.* [39].

Table 3.2: Mechanical and physical properties of rock specimens used in this study [39].

Rock name	**Tuffeau**	**Savonnieres**	**Mountain Gold**
Uni-axial compressive strength (MPa)	8.51	19.58	34
Elastic modulus (GPa)	1.70	12.23	8.10
Poisson's ratio	0.24	0.21	0.20
Dry porosity (%)	41.49	32.23	15.70
Dry density (Kg/m^3)	1360	1880	2220
Permeability (mD)	39.07	91.50	2.09

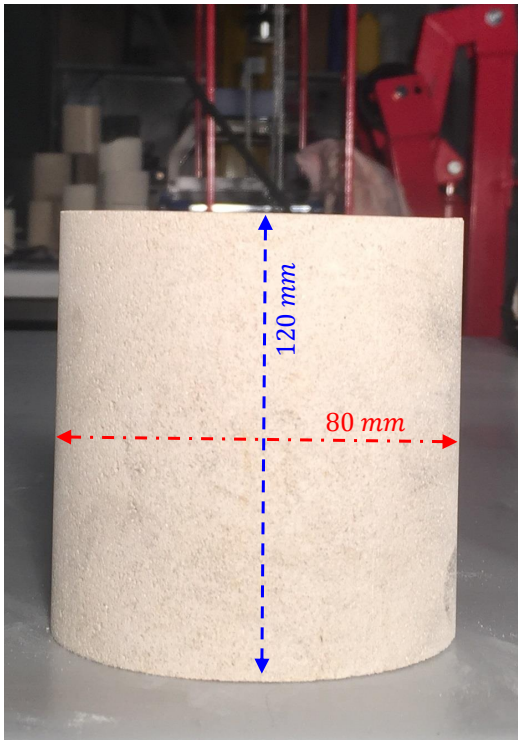


Figure 3.8: Dimensions of a rock specimen used for the scratch test.

Additional cylindrical plugs (38 mm in diameter and approximately 80 mm in length) were also extracted from the same rock blocks for further mechanical characterization under triaxial stress loading in the laboratory. The aims of these triaxial tests were: (i) to

determine the internal friction coefficient/angle for each rock specimen; and (*ii*) compare them to the friction coefficient/angle derived from the starch test.

To this end, several single-stage triaxial tests were carried out on multiple plugs under different confining pressures, i.e., at 2, 2.5, and 5 MPa for the Tuffeau limestone; 5, 10, and 15 MPa for the Mountain Gold sandstone. The triaxial experiments were conducted in Geomechanics and Geophysics Laboratory (CSIRO), using a Sanchez Technologies triaxial stress vessel [100–103]. Fig. 3.10 shows a schematic of the triaxial apparatus.

The multi-stage triaxial tests were conducted in a Sanchez Technologies triaxial stress vessel on cylindrical rock plugs 38 mm in diameter and up to 80 mm in length (see Fig. 3.9). This apparatus can apply a confining pressure up to 150 MPa, a pore pressure up to 100 MPa, and an axial load up to 700 KN [100–103].

The cylindrical rock plug was fit with a flexible Viton sleeve with top and bottom steel platens in order to: (*i*) isolate the sample from the confining medium (hydraulic oil); and (*ii*) apply an independent axial stress. The radial deformation of the rock plug within the horizontal plane is measured with a C-shaped cantilever made of brass and equipped with conventional strain gauges (resolution of the order of 1 micrometer). It is directly attached to two diametrically-opposite points on the lateral surface of the specimen through the Viton sleeve, and located at mid-height of the plug. The axial (vertical) displacement between the top and bottom platens is recorded with three contactless Eddy-current displacement sensors located outside the stress vessel, 120° apart within the horizontal plane (μ-Epsilon sensor DT3010-U15-M-C3 with a nominal resolution of 0.75 micrometer). The recorded displacement and the original length of the rock specimen were used to calculate the corresponding average axial deformation of the specimen. The control of the triaxial apparatus, the live monitoring of the test parameters, and the data acquisition were computerized through in-house software developed in the LabVIEW environment.

Additional features are available in this triaxial apparatus, which were not used in the work presented here. As such, these features are only briefly listed here for the sake of completeness, but not detailed, i.e., (*i*) heating up to 150°C, (*ii*) separate top and bottom pore fluid pumps and fluid pressure control/monitoring lines (up to 100 MPa), for conducting fluid injection/withdrawal or permeability experiments; and (*iii*) provision for a set of piezoceramic-based ultrasonic transducers that can act either as a sonic source or as a receiver. Up to 20 transducers can be simultaneously attached to the lateral surface of same rock plug through a specifically-moulded Viton sleeve. These transducers can be used for active ultrasonic monitoring (determination of elastic wave velocities), or for passive micro-seismic monitoring (acoustic emissions).

To prevent the confining oil from invading the sample and its pore space, the radial

strain and ultrasonic transducers penetrate the flexible Viton sleeve through collared holes moulded in the Viton sleeve with an embedded internal O-ring. In addition, to further minimize oil leakage risks and better tighten the internal contact between the transducers and the sleeve, an additional external O-ring is set around each hole collar.

Stress and strain data were recorded during each loading stage and used to conduct a Coulomb failure analysis, and determine the internal friction angle/coefficient for each rock specimen. In practice, the internal friction angle (φ) is the slope of the tangent to the Mohr circles for all confining pressures (see Fig. 3.11 and Fig. 3.12). We obtained $\varphi = 26.2°$ for the Tuffeau, and $\varphi = 32.4°$ for the Mountain Gold. The internal friction angle for the Savonnieres limestone through triaxial tests on the polyaxial press was reported by Dagrain [93], i.e., $\varphi = 37.9°$. The tests were carried out on cubic rock specimens with a 30 mm edge at the Rock Mechanics Laboratory of the Polytechnic Faculty of Mons.

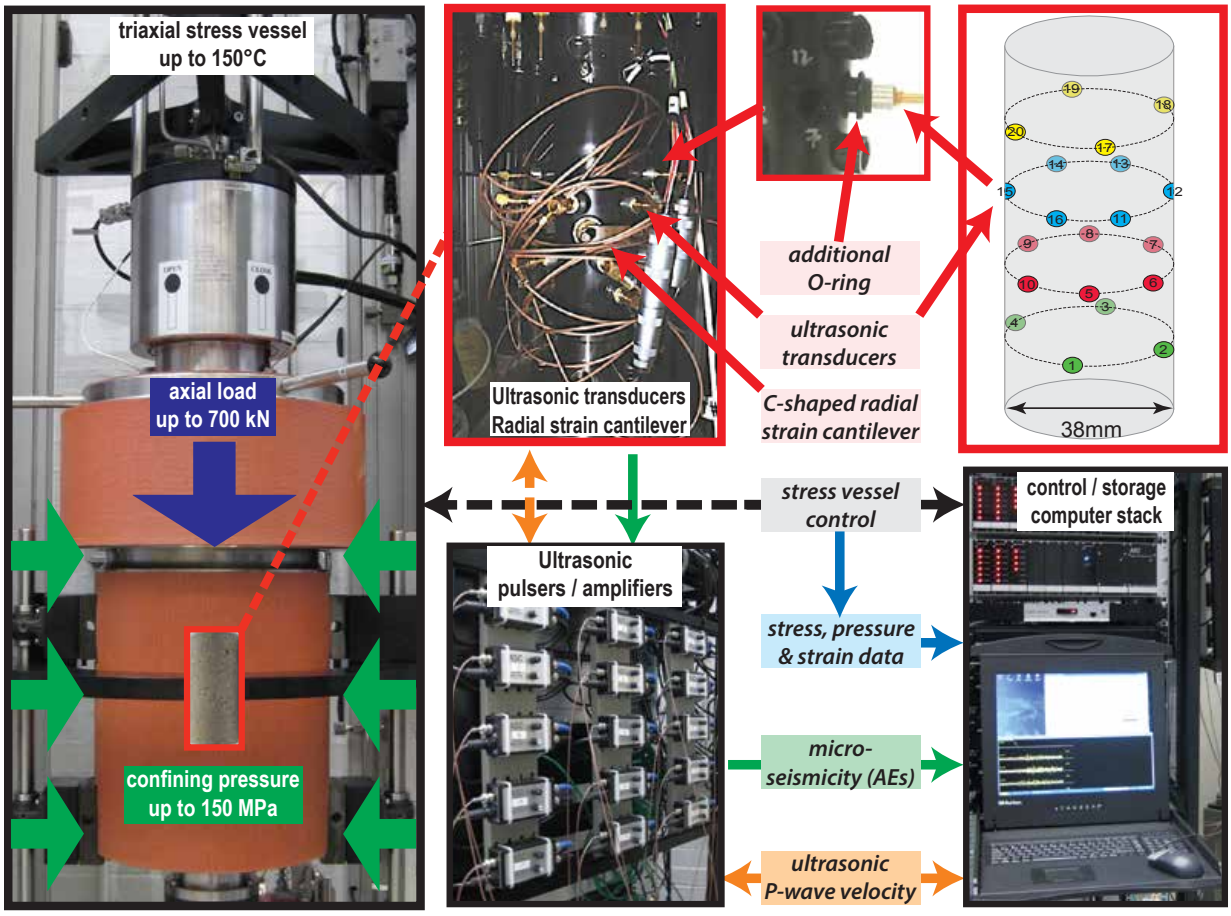


Figure 3.9: Functional representation of the Sanchez Technologies triaxial stress vessel available at Geomechanics and Geophysics Laboratory (modified from Sarout *et al.* [102]).

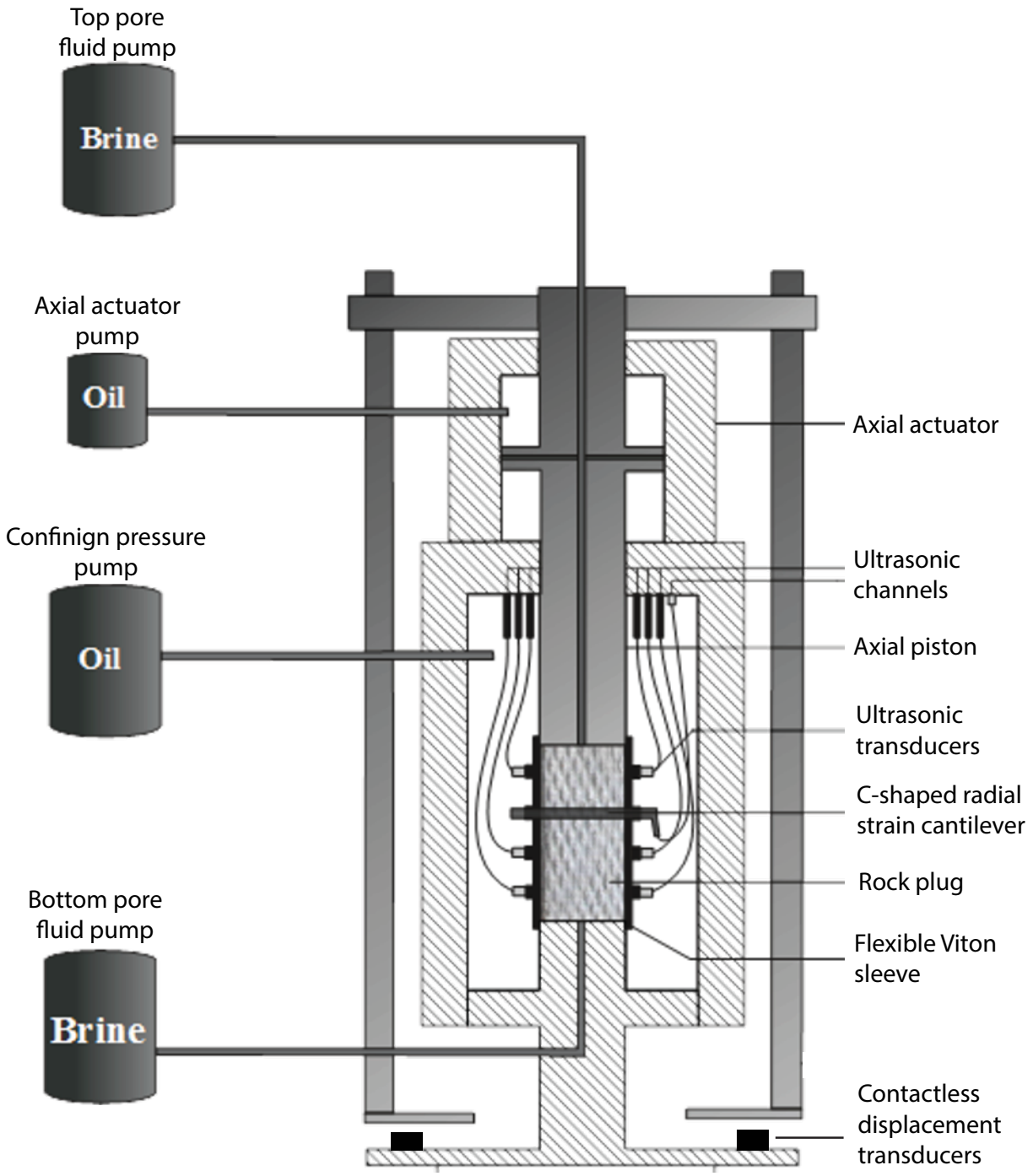


Figure 3.10: Schematic representation of the Sanchez Technologies triaxial stress vessel (modified from Velcin *et al.* [103]).

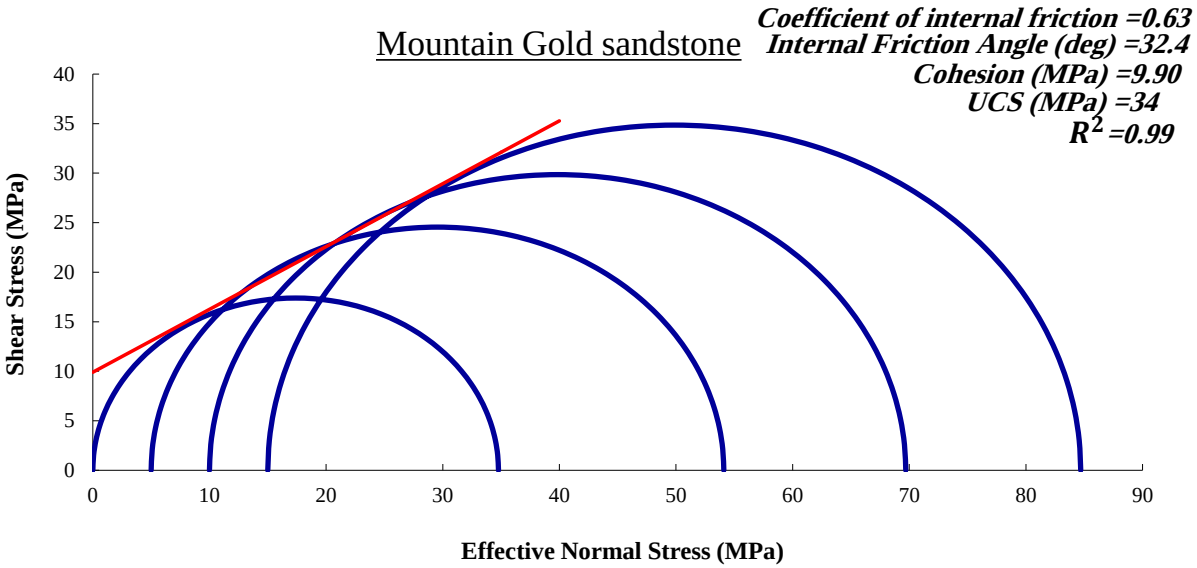


Figure 3.11: Plot of shear stress versus effective normal stress. Tests conducted on Mountain Gold sandstone.

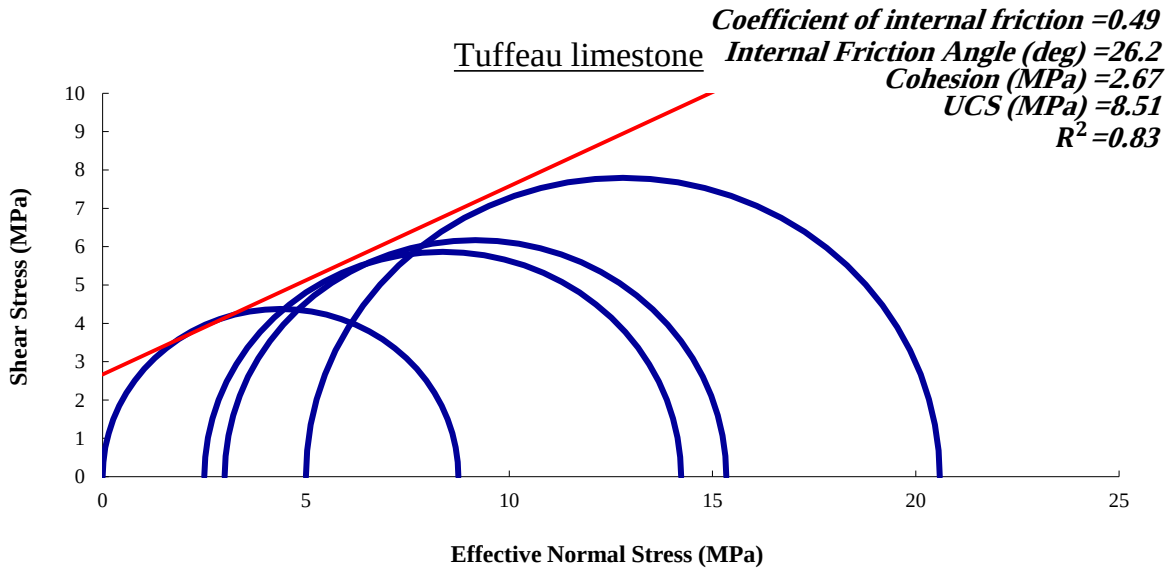


Figure 3.12: Plot of shear stress versus effective normal stress. Tests conducted on Tuffeau limestone.

Chapter 4

Results and Discussion

In order to explore the relationship between the apparent friction angle (ϕ) and the internal friction angle (φ), a series of single PDC cutting tests was conducted on three quarry rock specimens (Mountain Gold, Tuffeau, and Savonnieres) using a blunt cutter at different inclination angles of the wear flat surface ranging from 0° to roughly 15° and different cutting depths ranging from 0.10 mm to 0.90 mm with an interval of 0.10 mm. The magnitudes of the internal friction angles (φ) were estimated from the TC tests (section 3.4) and the apparent friction angles (ϕ) obtained from the scratch tests are compared.

4.1 Determination of internal friction angle

Fig. 4.1 to Fig. 4.3 show the evolutions of the apparent friction coefficient at the wear flat-rock interface as well as the apparent friction angle as a function of inclination angle obtained from the scratch tests conducted on two fine grain limestones (Tuffeau and Savonnieres) and one coarse-grained sandstone (Mountain Gold). As clearly shown, the inclination angle (β) of the wear flat has a pronounced effect on both the apparent friction coefficient mobilized at the wear flat-rock interface as well as the apparent friction angle. The evolution of the apparent friction angle shown in these figures clearly shows that the apparent friction angle, in which the inclination angle of the wear flat surface is equal to 0° or is parallel to the free surface of the rock being cut, is comparable with the internal friction angle (φ) of the tested rock specimens, which can be estimated by approximating the failure envelope (is non-linear) and 3.12) obtained through TC tests, to a linear Coulomb envelope, as shown in Fig. 3.11 and Fig. 3.12. Therefore, it can be concluded that the

scratch test can be an alternative approach to measure the internal friction angle of the intact rock specimens when $\beta = 0°$, see Table 4.1.

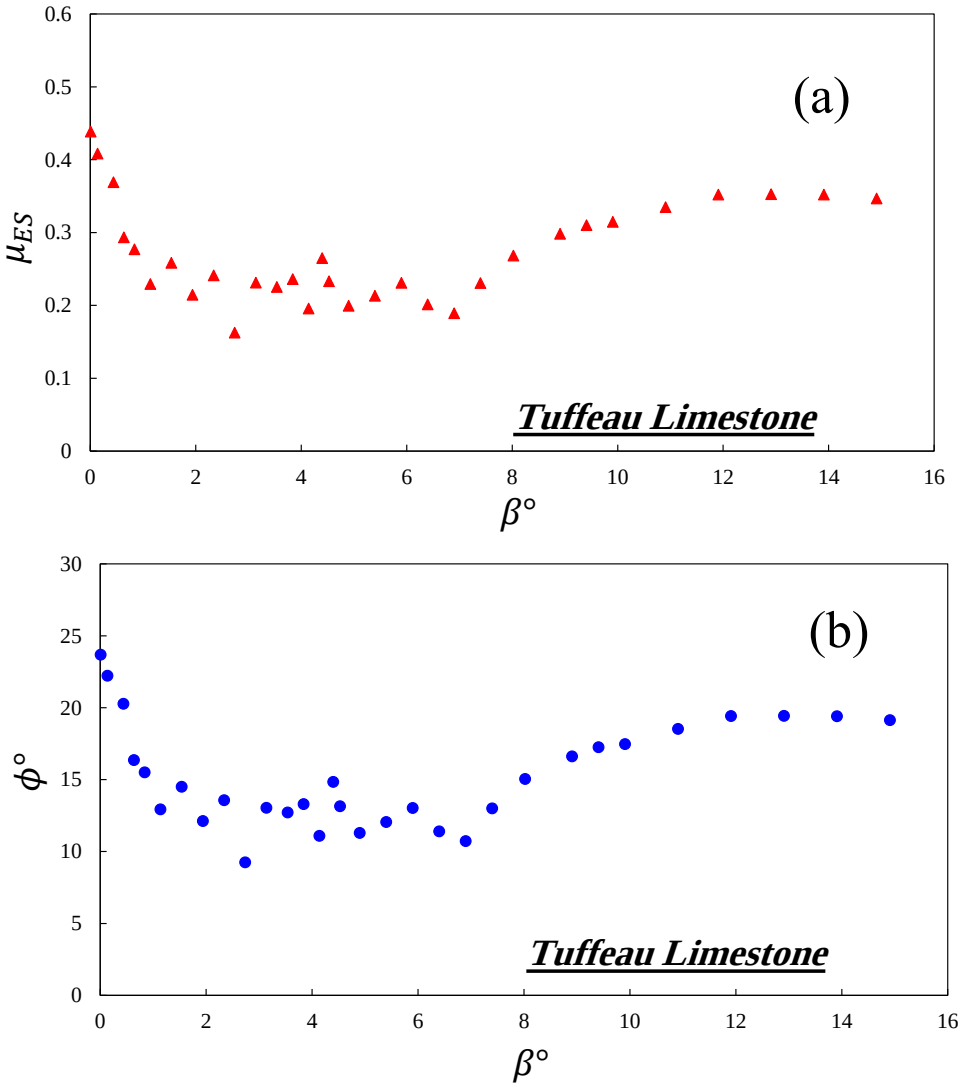


Figure 4.1: Plot of (a) apparent friction coefficient (μ_{ES}) and, (b) apparent friction angle (ϕ) as a function of inclination angle (β). Tests conducted on Tuffeau limestone using blunt cutter *5B*.

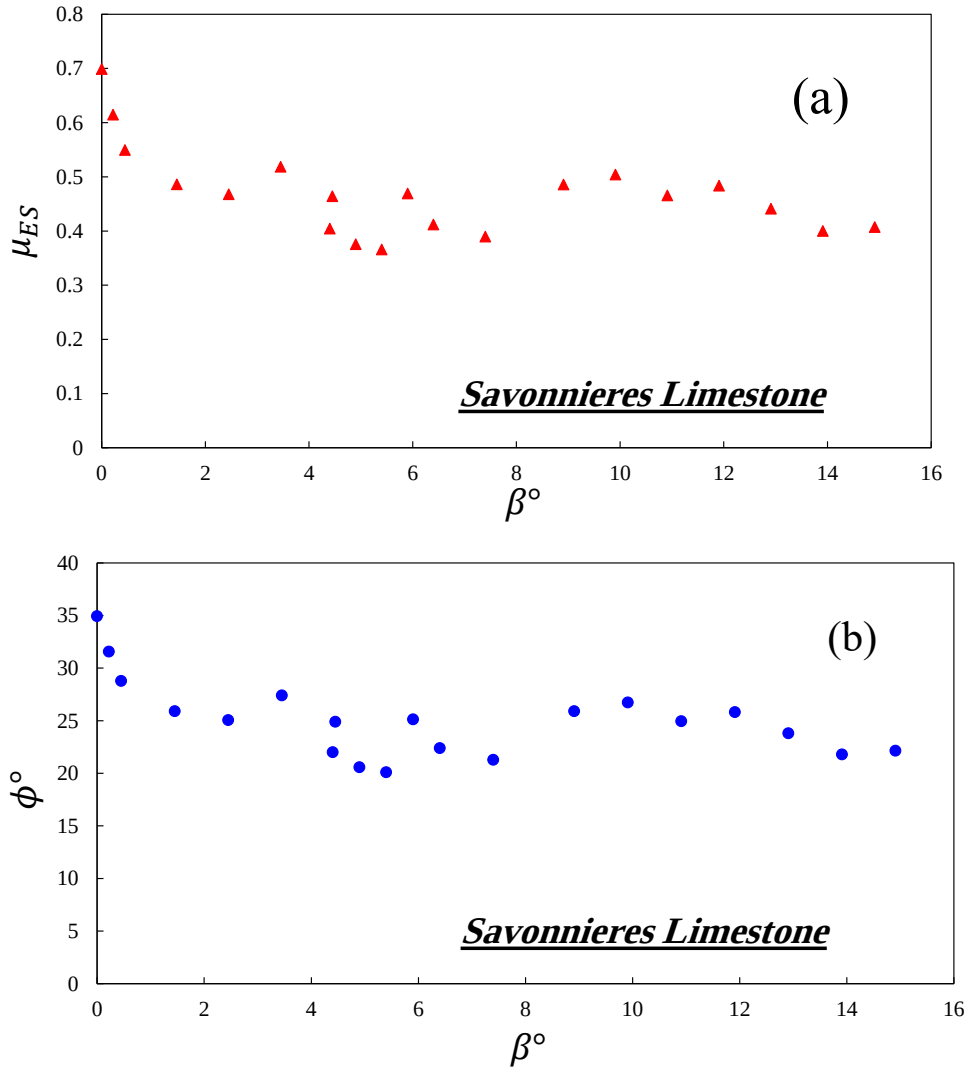


Figure 4.2: Plot of (a) apparent friction coefficient (μ_{ES}) and, (b) apparent friction angle (ϕ) as a function of inclination angle (β). Tests conducted on Savonnieres limestone using blunt cutter $5B$.

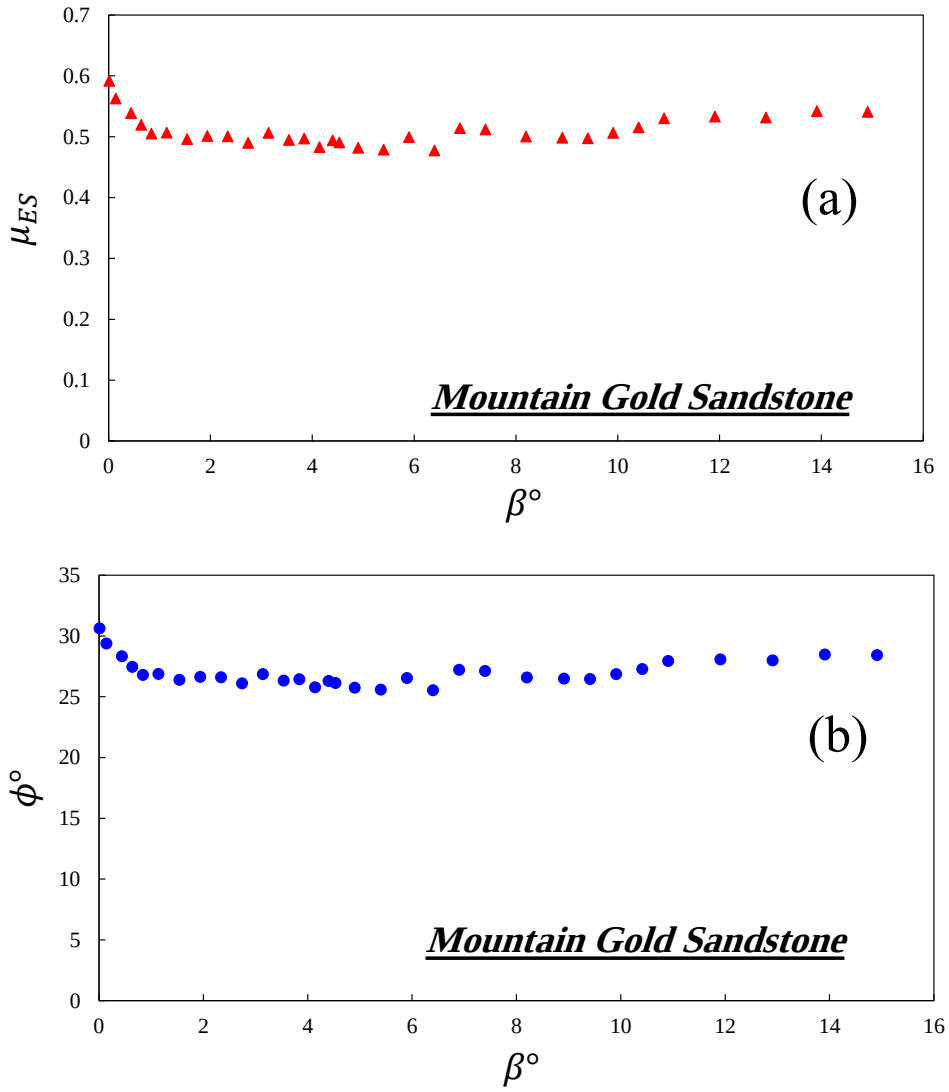


Figure 4.3: Plot of (a) apparent friction coefficient (μ_{ES}) and, (b) apparent friction angle (ϕ) as a function of inclination angle (β). Tests conducted on Mountain Gold sandstone using blunt cutter $5B$.

Table 4.1: Comparison between the internal friction angle (φ) estimated from triaxial (TC) tests and the apparent friction angle (ϕ) of rock specimens obtained from scratch tests when $\beta = 0°$.

Rock name	$\varphi°$	$\phi°$
Mountain Gold	32.40°	32.50°
Tuffeau	26.20°	24.23°
Savonnieres	37.95°	36.27°

The experimental results have been conceptually explained by the presence of a boundary layer of loose grains and pulverized rock particles between the wear flat and the rock mentioned by Chaput [52]. In practice, crushed rock is formed in front of the cutter while the rock is being cut and part of the cuttings flow upwards freely while the rest of the cutting particles flow underneath the cutter and form a boundary layer between the wear flat and rock surface, as schematically shown in Fig. 2.12. Likewise, Fig. 4.4 reveals the experimental observations of the boundary layers generated after the cutting tests conducted on Mountain Gold sandstone using a blunt PDC cutter at two different cutting depths; 0.20 mm and 0.80 mm. In other words, crushed rock is formed continuously in a small zone (one to three grains thick) ahead of the tip of the PDC cutter, and while part of the crushed material is removed by the cutter and flows upwards, another part stays under the cutter, forming the layer over which the wear flat slides, as shown in Fig. 2.12. In fact, the apparent friction coefficient (μ_{ES}) at the wear flat-rock interface of the blunt PDC cutting tool could reflect the frictional properties of this layer of pulverized rock and loose grains under conditions of high stress at the wear flat-rock interface [37]. As a consequence, the experimental results show that the apparent friction that is observed in the scratch test with the PDC blunt cutters does correlate with the internal friction angle of the rock specimen, hence allowing this property to be measured by a simpler test than more complex procedures such as the TC testing.

In conclusion, experimental observations indicate that the apparent friction coefficient at the wear flat-rock interface is similar to the frictional properties of this boundary layer which is consistent with the results of Adachi [88] and Lhomme [92]. However, new findings of this study also indicate that this correlation is only valid when the inclination angle (β) of the wear flat surface of the blunt PDC cutter is positioned at or very close to zero degrees, as already shown in Figs. 4.1 to 4.3 and schematically depicted in Fig. 2.12. Thus, the results imply that the inclination angle of the wear flat surface must be set carefully, as any small error can lead to considerable differences in the derived value of the internal friction angle. As a consequence, the experimental results imply that to measure

the internal friction angle using a scratch test, the wear flat surface of the blunt cutter must be set parallel to the free surface of the rock specimen being cut.

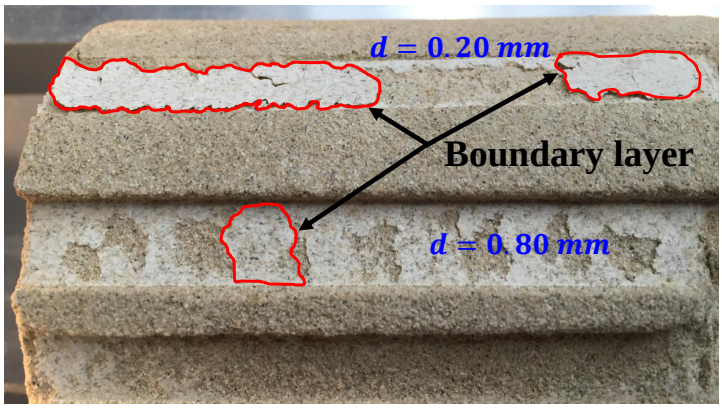


Figure 4.4: Boundary layer of crushed rocks after scratch tests at two different depths of cut (d). Test conducted with a blunt PDC cutter on Mountain Gold sandstone.

As already mentioned, it is observed in Fig. 4.1 to Fig. 4.3 that the apparent friction coefficient varies with the inclination angle (β) of the wear flat surface. One possible explanation is that the number of the grains in contact with the wear flat surface (flowing backward underneath the cutting tool) varies with inclination angle β (or the back rake angle θ), which in turn, results in different thicknesses of the boundary layer of the pulverized rock (loose particles). In addition, the grain size has a remarkable effect on the measured apparent friction coefficient. In the case of Savonnieres limestone with the smallest grain size [39, 104, 105], the wear flat of blunt cutter *5B* was observed under a scanning electron microscope (SEM) after the cutting process, see Fig. 4.5. As can be seen in Fig. 4.6, the results of the material concentration plot shows the presence of a high amount of Silicon (Si) which is a rock element in the asperities of the wear flat which is well consistent with the findings of Dagrain [93] and Borgaonkar [104]. The scanning image of the wear flat implies that the cuttings adhere to the PDC wear flat along the cutting process at all inclination angles, as schematically depicted in Fig. 4.7. From the results of this section, it can be concluded that the apparent friction coefficient (as well as the apparent friction angle) is not only a rock property but also is a function of cutter wear flat inclination angle and the grain size.

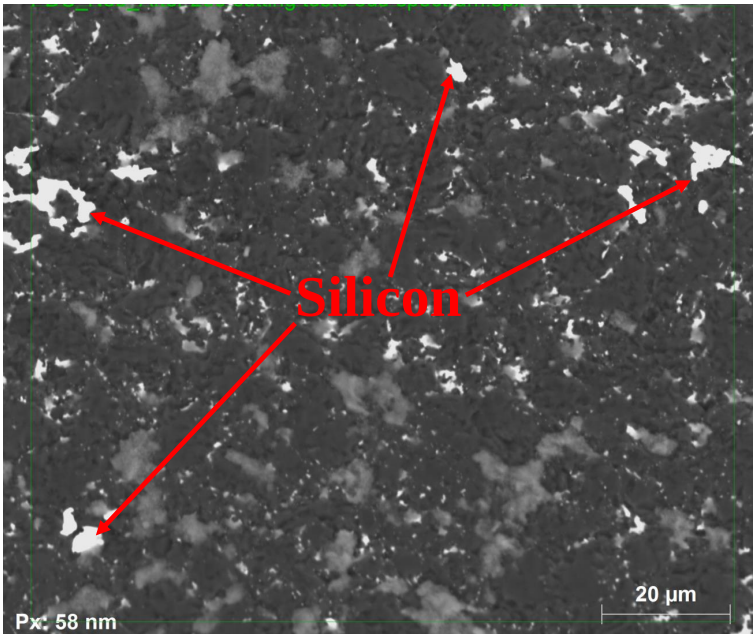


Figure 4.5: Scanning electron photo of the wear flat surface of the blunt cutter using Secondary Electron Microscope (SEM).

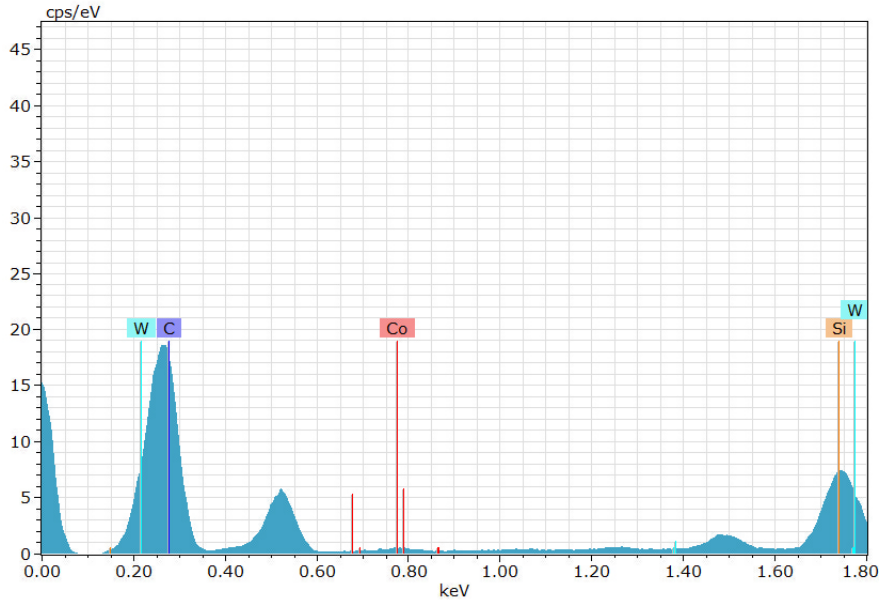


Figure 4.6: Material concentration plot in Counts Per Second (cps) versus Electron-Volt (ev) obtained by the SEM. Tests conducted on Savonnieres limestone. Si: Silicon, W: Tungsten, C: Carbon, and Co: Cobalt.

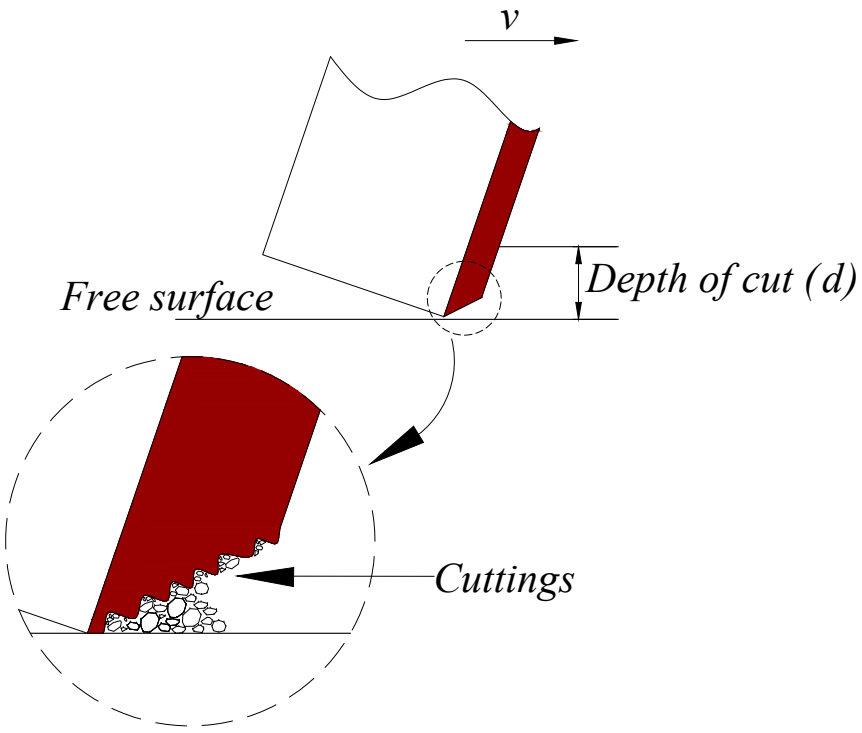


Figure 4.7: Schematic of cuttings trapped on the wear flat surface in rock cutting at a constant depth of cut (d).

4.2 Effect of wear flat properties on apparent friction angle

Scratch tests were conducted on two rock specimens with the five blunt PDC cutters *5B* ($R_a = 0.38\ \mu m$), *5D* ($R_a = 0.87\ \mu m$), *M1* ($R_a = 0.65\ \mu m$), *M2* ($R_a = 0.98\ \mu m$), and *M3* ($R_a = 1.42\ \mu m$) characterized with similar wear flat inclination angle but different roughness of wear flat surface. In addition, one blunt carbide cutter was also used to investigate the effect of wear flat material on the apparent friction coefficient.

Fig. 4.8 and Fig. 4.9 demonstrate the influence of wear flat roughness (R_a) on the apparent friction coefficient (μ) and the apparent friction angle (ϕ). It is obvious that an

increase in wear flat roughness is accompanied by a slight increase in the apparent friction coefficient. This result is also consistent with the results of Dagrain [93] and Rostamsowlat [91]. Therefore, an increase of the apparent friction coefficient caused by an increase in the wear flat roughness leads to an increase in the derived apparent friction angle [88, 91–93]. As a consequence, it can be concluded that variations in the wear flat roughness is accompanied by variations in the associated internal friction angle of the tested rock specimen. The available data for other rock types [40, 91], however, show similar behavior to those of Fig. 4.8 and Fig. 4.9; but are not included here for brevity.

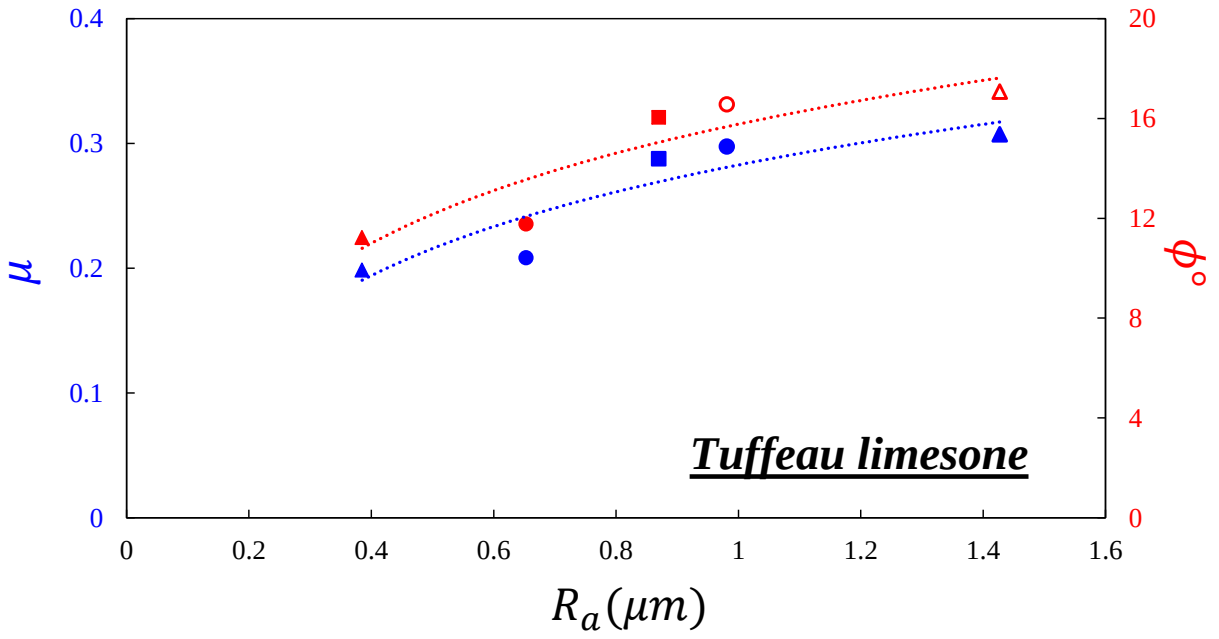


Figure 4.8: Evolution of apparent friction coefficient (μ) and apparent friction angle (ϕ) versus wear flat roughness (R_a). Tests conducted on Tuffeau limestone when $\beta = 1.18°$.

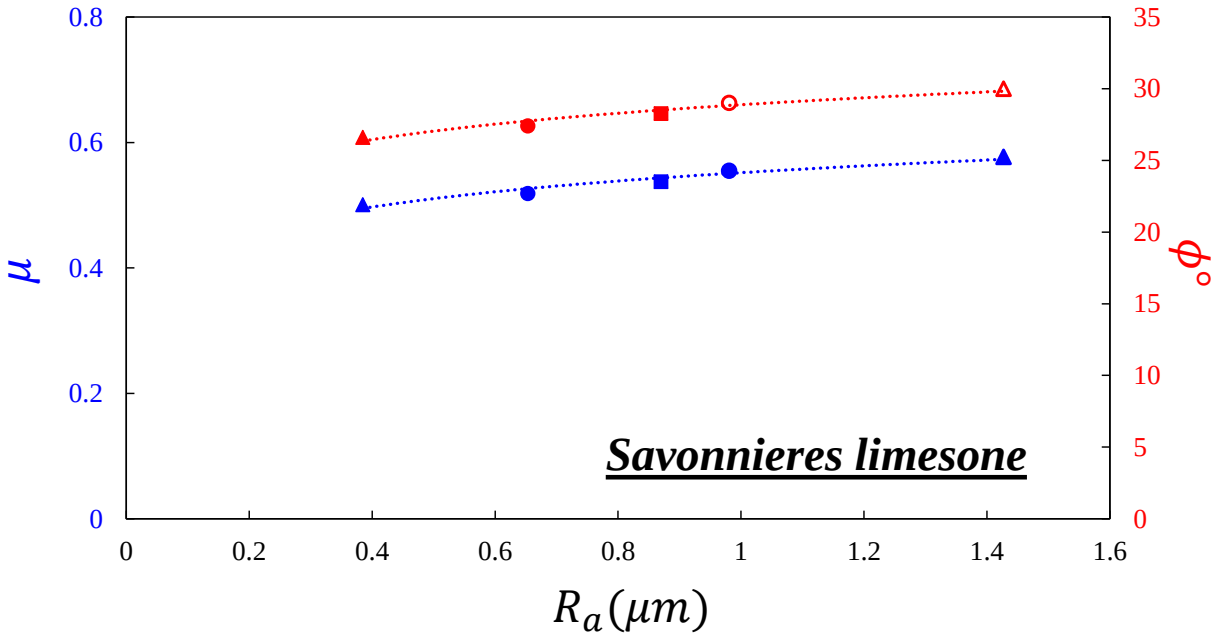


Figure 4.9: Evolution of friction coefficient (μ) and friction angle (ϕ) versus wear flat roughness (R_a). Tests conducted on Savonnieres limestone when $\beta = 9.70°$.

A series of scratch tests was carried out on relatively fine grained Tuffeau limestone and Savonnieres limestone using the blunt PDC cutter *5B* and the carbide blunt cutter. These blunt cutters are characterized by different wear flat materials, as mentioned in section 3.3. Note that the cutting tests were not conducted on Mountain Gold sandstone due to the rock abrasiveness, which resulted in wearing out the carbide cutter immediately. The results of apparent friction coefficient versus inclination angle for cutters with different wear flat materials are plotted in Fig. 4.10 and Fig. 4.11. The results show that the wear flat material has a significant effect on the apparent friction coefficient mobilized at the wear flat-rock interface. The results of cutting tests [91] with different amounts of carbide to PDC in the wear flat surface suggested that an increase in the level of carbide material in the wear flat surface of a blunt cutting tool leads to an increase in the wear flat roughness, which in turn, results in an increase of the apparent friction coefficient, in particular, for small and moderate inclination angles of the wear flat surface. As a consequence, the cutting performance of blunt cutting tools to measure the friction coefficient is predominantly affected by the wear flat material or, more specifically, the

wear flat roughness.

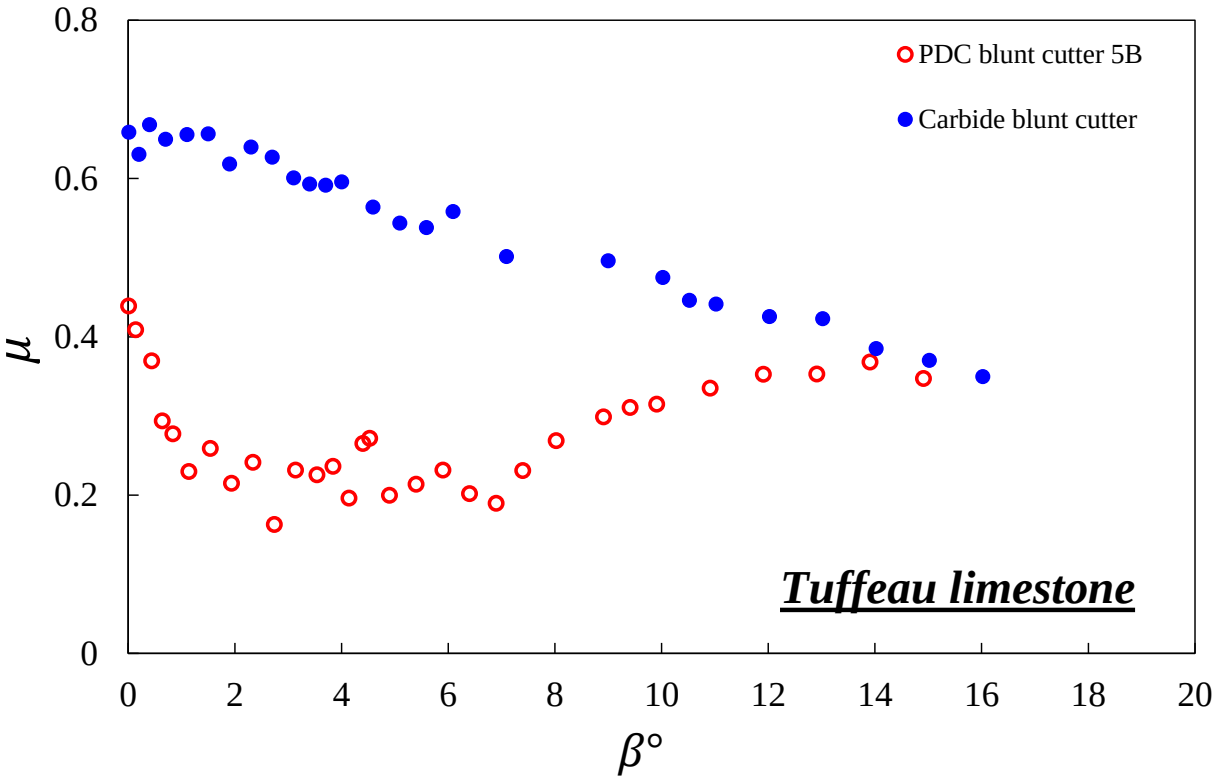


Figure 4.10: Plot of apparent friction coefficient as a function of inclination angle. Tests conducted on Tuffeau limestone with *carbide* cutter and PDC cutter *5B*.

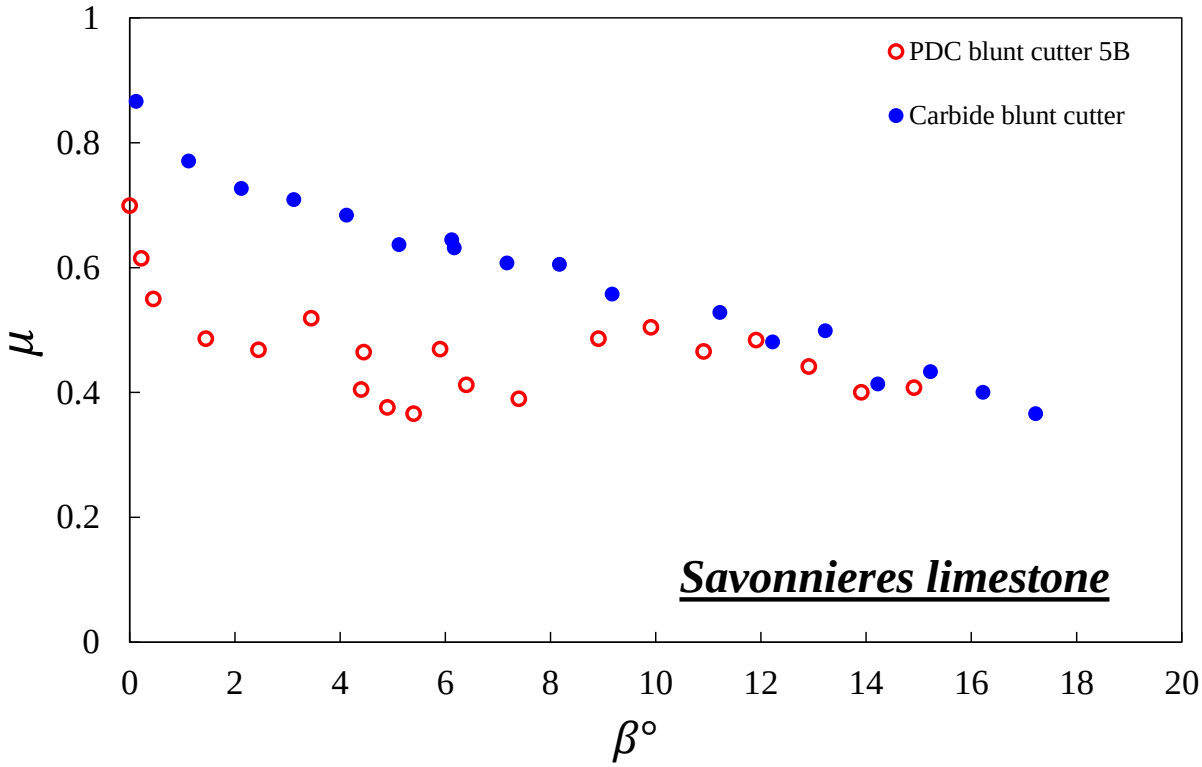


Figure 4.11: Plot of apparent friction coefficient as a function of inclination angle. Tests conducted on Savonnieres limestone with *carbide* cutter and PDC cutter *5B*.

Chapter 5

Conclusion and Future Work

The present study was designed to determine the apparent friction angle between PDC bits and rock as well as finding the relationship between the internal friction angle and the apparent friction angle of the intact rock specimens using a scratch test. For this purpose, a series of rock cutting tests using a blunt PDC cutter with different inclination angles of the wear flat surface was performed on two limestones (Savonnieres and Tuffeau) and one coarse-grained sandstone (Mountain Gold). Furthermore, various blunt cutters with different wear flat roughness and different wear flat materials were used to investigate the effect of wear flat properties on the apparent friction coefficient and eventually the measured apparent friction angle.

The findings of this study have provided experimental evidence that the apparent friction coefficient at the wear flat-rock interface underneath the cutter is actually a property of the layer of loose rock particles (under specific testing conditions). Also, the internal friction angle of rock can be assessed from a scratch test using a relatively polished blunt PDC cutter when the inclination angle of the wear flat surface is set to zero degrees and the cutting tests are carried out within the ductile regime of failure under atmospheric pressure and dry conditions. The conceptual explanation for this relationship between the friction angle and the internal friction angle is based on experimental evidence suggesting the existence of a layer of loose rock particles at the tool-rock interface. This layer is formed due to the result of the crushing of rock grains below the wear flat during the cutting action.

The results of the experiments using blunt cutters with different roughness and materials suggest that the measured apparent friction coefficient at the wear flat-rock interface and eventually the apparent friction angle is affected by the wear flat properties. This vari-

ation is more pronounced with cutters with different wear flat materials. The experimental findings of this research suggest that rock cutting using a PDC cutter with a polished wear flat surface (or minimum roughness) can be an appropriate choice to estimate the internal friction angle of the rock specimens. Likewise, comparison of the results of a PDC cutter with a carbide cutter showed that the estimated friction angle (the apparent friction angle) of rock increases due to an increase in the level of the carbide material at the contact surface.

The main outcome of this research study is that the scratch test can be considered as an alternative approach to measure the internal friction angle of rocks under specific testing conditions as the scratch test possesses some advantages over the triaxial test. Further, the apparent friction coefficient (and eventually the apparent friction angle) obtained from a scratch test is a function of wear flat inclination angle, wear flat roughness, wear flat material, and the rock grain size.

Recommendations for future research:

1. *Measurement of the hardness.* It could be of interest to run indentation test on the same rock samples to measure the hardness and compare with the contact stress derived from cutting tests. The motivation for such work is the postulation that the contact stress is comparable with rock hardness when the regime of frictional contact occurs within the elastoplastic regime.

2. *Numerical modeling.* Further numerical simulations could be carried out to explore how the friction coefficient could affect the response in the elastic regime. It would also be interesting to model both the cutting and contact process and explore how they affect each other (possibly with code such as PFC).

References

[1] C. Chang, M. D. Zoback, and A. Khaksar, "Empirical relations between rock strength and physical properties in sedimentary rocks," *Journal of Petroleum Science and Engineering*, vol. 51, no. 3-4, pp. 223–237, 2006.

[2] T. Richard, F. Dagrain, E. Poyol, and E. Detournay, "Rock strength determination from scratch tests," *Engineering Geology*, vol. 147-148, pp. 91–100, 2012.

[3] C. Lakshminarayana, A. K. Tripathi, and S. K. Pal, "Estimation of rock strength properties using selected mechanical parameters obtained during the rotary drilling," *Journal of The Institution of Engineers (India): Series D*, pp. 1–10, 2019.

[4] J. Franklin, E. Broch, and G. Walton, "Logging the mechanical character of rock," 1971.

[5] Z. T. Bieniawski, "The point-load test in geotechnical practice," *Engineering Geology*, vol. 9, no. 1, pp. 1–11, 1975.

[6] T. Szwedzicki, "Indentation hardness testing of rock," *International Journal of Rock Mechanics and Mining Sciences*, vol. 35, no. 6, pp. 825–829, 1998.

[7] T. Richard, E. Detournay, A. Drescher, P. Nicodeme, and D. Fourmaintraux, "The scratch test as a means to measure strength of sedimentary rocks," No. SPE 47196, (Trondheim, Norway), pp. 1–8, SPE/ISRM Eurock 98, Society of Petroleum Engineers, July 1998.

[8] J. Rusnak and C. Mark, "Using the point load test to determine the uniaxial compressive strength of coal measure rock," pp. 362–371, Proceedings of the 19th International Conference on Ground Control in Mining. Morgantown, WV: West Virginia University, 2000.

[9] A. Aydin and A. Basu, "The Schmidt hammer in rock material characterization," *Engineering Geology*, vol. 81, no. 1, pp. 1–14, 2005.

[10] J. H. Dieterich, "Modeling of rock friction: 1. experimental results and constitutive equations," *Journal of Geophysical Research: Solid Earth*, vol. 84, no. B5, pp. 2161–2168, 1979.

[11] E. Lajtai and A. Gadi, "Friction on a granite to granite interface," *Rock mechanics and rock engineering*, vol. 22, no. 1, pp. 25–49, 1989.

[12] ASTM, "Standard test method for triaxial compressive strength of undrained rock core samples without pore pressure measurements," vol. American Society for Testing and Materials (ASTM), pp. D2664–95a, 1996.

[13] T. Ramamurthy, "Shear strength response of some geological materials in triaxial compression," *International Journal of Rock Mechanics and Mining Sciences*, vol. 38, no. 5, pp. 683–697, 2001.

[14] G. Barla, M. Barla, and M. Martinotti, "Development of a new direct shear testing apparatus," *Rock Mechanics and Rock Engineering*, vol. 43, no. 1, pp. 117–122, 2010.

[15] H. Konietzky, T. Frühwirt, and H. Luge, "A new large dynamic rockmechanical direct shear box device," *Rock Mechanics and Rock Engineering*, vol. 45, no. 3, pp. 427–432, 2012.

[16] G. Wang, Y.-s. PAN, X.-c. XIAO, G.-y. CHEN, and L.-p. DAI, "Experimental study on the charge induction regularity in the shearing process of coal [j]," *Journal of Safety and the Environment*, vol. 16, no. 3, pp. 103–108, 2016.

[17] F.-Q. Gong, X.-F. Si, X.-B. Li, and S.-Y. Wang, "Dynamic triaxial compression tests on sandstone at high strain rates and low confining pressures with split hopkinson pressure bar," *International Journal of Rock Mechanics and Mining Sciences*, vol. 113, pp. 211–219, 2019.

[18] F. Gong, S. Luo, G. Lin, and X. Li, "Evaluation of shear strength parameters of rocks by preset angle shear, direct shear and triaxial compression tests," *Rock Mechanics and Rock Engineering*, pp. 1–15, 2020.

[19] J. C. Jaeger, N. G. Cook, and R. Zimmerman, *Fundamentals of rock mechanics*. John Wiley & Sons, 2009.

[20] H.-S. Jang, Q.-Z. Zhang, S.-S. Kang, and B.-A. Jang, "Determination of the basic friction angle of rock surfaces by tilt tests," *Rock Mechanics and Rock Engineering*, vol. 51, no. 4, pp. 989–1004, 2018.

[21] B. Tiryaki, "Predicting intact rock strength for mechanical excavation using multivariate statistics, artificial neural networks, and regression trees," *Engineering Geology*, vol. 99, no. 1-2, pp. 51–60, 2008.

[22] B. R. Kumar, H. Vardhan, and M. Govindaraj, "Sound level produced during rock drilling vis-à-vis rock properties," *Engineering geology*, vol. 123, no. 4, pp. 333–337, 2011.

[23] B. Akbari, S. Miska, M. Yu, and R. Rahmani, "The effects of size, chamfer geometry, and back rake angle on frictional response of PDC cutters," 48th US Rock Mechanics / Geomechanics Symposium held in Minneapolis, MN, USA, ARMA, 2014.

[24] S. Kahraman, O. Toraman, and S. Cayirli, "Predicting the strength and brittleness of rocks from a crushability index," *Bulletin of Engineering Geology and the Environment*, vol. 77, no. 4, pp. 1639–1645, 2018.

[25] E. Detournay, A. Drescher, D. Fourmaintraux, and P. Defourny, "Assessment of rock strength properties from cutting tests: Preliminary experimental evidence," (Brussels, Belgium), pp. 1–10, Proceedings of the Colloquium Mundanum on Chalk and Shales, 1995.

[26] J. I. Adachi, E. Detournay, and A. Drescher, "Determination of rock strength parameters from cutting tests," *Proc. NARMS*, pp. 1517–1523, 1996.

[27] H. Munoz, A. Taheri, and E. Chanda, "Rock cutting characteristics on soft-to-hard rocks under different cutter inclinations," *International Journal of Rock Mechanics and Mining Sciences*, vol. 87, pp. 85–89, 2016.

[28] I. Rostamsowlat, T. Richard, and B. Evans, "An experimental study of the effect of back rake angle in rock cutting," *International Journal of Rock Mechanics and Mining Sciences*, vol. 107, pp. 224–232, 2018.

[29] T. M. Warren and L. A. Sinor, "PDC bits: what's needed to meet tomorrow's challenge," University of Tulsa Centennial Petroleum Engineering Symposium, 29-31 August, Tulsa, Oklahoma, Society of Petroleum Engineers, August 1994.

[30] M. Sneddon and D. Hall, "Polycrystalline diamond: manufacture, wear mechanisms, and implications for bit design," *Journal of Petroleum Technology*, vol. 40, no. 12, pp. 1593–1601, 1988.

[31] L. Gerbaud, S. Menand, and H. Sellami, "PDC bits: All comes from the cutter rock interaction," IADC/SPE Drilling Conference, 21-23 February, Miami, Florida, USA, Society of Petroleum Engineers, 2006.

[32] E. Detournay, T. Richard, and M. Shepherd, "Drilling response of drag bits: Theory and experiment," *International Journal of Rock Mechanics and Mining Sciences*, vol. 45, no. 8, pp. 1347–1360, 2008.

[33] Y. Ma, Z. Huang, Q. Li, Y. Zhou, and S. Peng, "Cutter layout optimization for reduction of lateral force on PDC bit using kriging and particle swarm optimization methods," *Journal of Petroleum Science and Engineering*, vol. 163, pp. 359–370, April 2018.

[34] A. Ghasemloonia, D. G. Rideout, and S. D. Butt, "A review of drillstring vibration modeling and suppression methods," *Journal of Petroleum Science and Engineering*, vol. 131, pp. 150–164, 2015.

[35] F. Bellin, A. Dourfaye, W. King, and M. Thigpen, "The current state of PDC bit technology," *World oil*, vol. 231, no. 9, 2010.

[36] I. Rostamsowlat, B. Evans, and H. J. Kwon, "A review of the frictional contact in rock cutting with a pdc bit," *Journal of Petroleum Science and Engineering*, vol. 208, p. 109665, 2022.

[37] E. Detournay and P. Defourny, "A phenomenological model for the drilling action of drag bits," *International Journal of Rock Mechanics and Mining Sciences & Geomechanics Abstracts*, vol. 29, no. 1, pp. 13–23, 1992.

[38] I. Rostamsowlat, B. Akbari, and B. Evans, "Analysis of rock cutting process with a blunt pdc cutter under different wear flat inclination angles," *Journal of Petroleum Science and Engineering*, vol. 171, pp. 771–783, 2018.

[39] I. Rostamsowlat, T. Richard, and B. Evans, "Experimental investigation on the effect of wear flat inclination on the cutting response of a blunt tool in rock cutting," *Acta Geotechnica*, vol. 14, no. 2, pp. 519–534, 2019.

[40] I. Rostam Sowlat, *Effect of cutter and rock properties on the frictional contact in rock cutting with blunt tools*. PhD thesis, Curtin University, 2017.

[41] J. Almenara and E. Detournay, "Cutting experiments in sandstones with blunt PDC cutters," pp. 215–220, Rock Characterization: ISRM Symposium, Eurock'92, Chester, UK, 14–17 September 1992, Thomas Telford Publishing, 1992.

[42] J. F. Brett, T. M. Warren, S. M. Behr, *et al.*, "Bit whirl: A new theory of PDC bit failure," SPE Annual Technical Conference and Exhibition, Society of Petroleum Engineers, 1989.

[43] S. Menand, L. Gerbaud, and A. Dourfaye, "PDC bit technology improvements increase efficiency, bit life," *Drilling Contractor*, pp. 52–54, Mar. 2005.

[44] T. Richard, "Determination of rock strength from cutting tests," m. Sc Thesis, Faculty of the Graduate School of the University of Minnesota, Minneapolis, Minnesota, U.S.A., 1999.

[45] Y. Zhou and J. S. Lin, "On the critical failure mode transition depth for rock cutting," *International Journal of Rock Mechanics and Mining Sciences*, vol. 62, pp. 131–137, 2013.

[46] Y. Zhou and J.-S. Lin, "Modeling the ductile-brittle failure mode transition in rock cutting," *Engineering Fracture Mechanics*, vol. 127, pp. 135 – 147, 2014.

[47] W. Liu, X. Zhu, and J. Jing, "The analysis of ductile-brittle failure mode transition in rock cutting," *Journal of Petroleum Science and Engineering*, 2017.

[48] R. Goodrich, "High pressure rotary drilling machines," No. 94 in Technical Series, (Rolla, Missouri, U.S.A.), pp. 25–45, Second Annual Symposium on Mining Research, Missouri School of Mines, November 1957.

[49] M. C. Jaime, Y. Zhou, J.-S. Lin, and I. K. Gamwo, "Finite element modeling of rock cutting and its fragmentation process," *International Journal of Rock Mechanics and Mining Sciences*, vol. 80, pp. 137–146, 2015.

[50] W. Liu and X. Zhu, "Experimental study of the force response and chip formation in rock cutting," *Arabian Journal of Geosciences*, vol. 12, no. 15, p. 457, 2019.

[51] P. A. Wawrzynek, "Discrete modeling of crack propagation: Theoretical aspects and implementation issues in two and three dimensions.," 1992.

[52] E. J. Chaput, "Observations and analysis of hard rocks cutting failure mechanisms using PDC cutters," tech. rep., London, United Kingdom, 1992.

[53] C. V. Min-Kwang Choi, Tae-Hwan Kim, "Fracture toughness test and its simulation for brittle and ductile steel," report, 2011.

[54] H. Huang and E. Detournay, "Intrinsic length scales in tool-rock interaction," *ASCE International Journal of Geomechanics*, vol. 8, no. 1, pp. 39–44, 2008.

[55] A.-T. Akono and F.-J. Ulm, "Scratch test model for the determination of fracture toughness," *Engineering Fracture Mechanics*, vol. 78, no. 2, pp. 334–342, 2011.

[56] H. Huang and E. Detournay, "Discrete element modeling of tool-rock interaction ii: rock indentation," *International Journal for Numerical and Analytical Methods in Geomechanics*, vol. 37, no. 13, pp. 1930–1947, 2013.

[57] H. Huang, B. Lecampion, and E. Detournay, "Discrete element modeling of tool-rock interaction i: rock cutting," *International Journal for Numerical and Analytical Methods in Geomechanics*, vol. 37, no. 13, pp. 1913–1929, 2013.

[58] J.-S. Lin and Y. Zhou, "Can scratch tests give fracture toughness?," *Engineering Fracture Mechanics*, vol. 109, pp. 161 – 168, 2013.

[59] Y. Zhou, *Numerical modeling of rock drilling with finite elements*. PhD thesis, University of Pittsburgh, 2013.

[60] A. T. Akono, F. J. Ulm, and Z. P. Bazant, "Discussion: Strength-to-fracture scaling in scratching," *Engineering Fracture Mechanics*, vol. 119, pp. 21 – 28, 2014.

[61] C. Fairhurst and W. Lacabanne, "Hard rock drilling techniques," *Mine Quarry Eng*, vol. 23, pp. 157–161, 1957.

[62] D. Zijsling, "Analysis of temperature distribution and performance of polycrystalline diamond compact bits under field drilling conditions," SPE annual technical conference and exhibition, 16-19 September, Houston, Texas, Society of Petroleum Engineers, 1984.

[63] D. A. Glowka, "Development of a method for predicting the performance and wear of PDC (polycrystalline diamond compact) drill bits," tech. rep., 1987.

[64] A. Wojtanowicz and E. Kuru, "Mathematical modeling of PDC bit drilling process based on a single-cutter mechanics," *Journal of Energy Resources Technology*, vol. 115, no. 4, pp. 247–256, 1993.

[65] N. Challamel and H. Sellami, "Application of yield design for understanding rock cutting mechanism," SPE/ISRM Rock Mechanics in Petroleum Engineering, Society of Petroleum Engineers, July 1998.

[66] R. Teale, "The concept of specific energy in rock drilling," *International Journal of Rock Mechanics and Mining Sciences & Geomechanics Abstracts*, vol. 2, no. 1, pp. 57–73, 1965.

[67] A. Naeimipour, J. Rostami, I. Buyuksagis, and O. Frough, "Estimation of rock strength using scratch test by a miniature disc cutter on rock cores or inside boreholes," *International Journal of Rock Mechanics and Mining Sciences*, vol. 107, pp. 9–18, 2018.

[68] P. Chen, M. Meng, S. Miska, M. Yu, E. Ozbayoglu, and N. Takach, "Study on integrated effect of pdc double cutters," *Journal of Petroleum Science and Engineering*, 2019.

[69] F. Dagrain, E. Poyol, and T. Richard, "Strength logging of geomaterials from scratch tests," (Salsbourg, Austria), EUROCK 2004 and 53rd Geomechanics Colloquium, October 2004.

[70] M. Theodoridou, F. Dagrain, and I. Ioannou, "Micro-destructive cutting techniques for the characterization of natural limestone," *International Journal of Rock Mechanics and Mining Sciences*, vol. 76, no. Supplement C, pp. 98 – 103, 2015.

[71] J. A. Mendoza, I. K. Gamwo, W. Zhang, and J. S. Lin, "Discrete element modeling of rock cutting using crushable particles," No. ARMA 10-232, (Salt Lake City, UT, U.S.A.), pp. 1–7, 44th US Rock Mechanics Symposium and 5th U.S.-Canada Rock Mechanics Symposium, American Rock Mechanics Association, June 2010.

[72] C. Coudyzer and T. Richard, "Influence of the back and side rake angles in rock cutting," pp. 5–7, AADE 2005 National Technical Conference and Exhibition, Wyndam Greenspoint, Houston, TX, April, 2005.

[73] W. Li, X. Ling, and H. Pu, "Development of a cutting force model for a single pdc cutter based on the rock stress state," *Rock Mechanics and Rock Engineering*, vol. 53, no. 1, pp. 185–200, 2020.

[74] G. Hareland, W. Yan, R. Nygaard, and J. L. Wise, "Cutting efficiency of a single PDC cutter on hard rock," *Journal of Canadian Petroleum Technology*, vol. 48, no. 6, pp. 60–65, 2009.

[75] S. Yadav, C. Saldana, and T. G. Murthy, "Experimental investigations on deformation of soft rock during cutting," *International Journal of Rock Mechanics and Mining Sciences*, vol. 105, pp. 123–132, 2018.

[76] R. Majidi, S. Z. Miska, and S. Tammineni, "Pdc single cutter: the effects of depth of cut and rpm under simulated borehole conditions," *Wiertnictwo, Nafta, Gaz*, vol. 28, no. 1-2, pp. 283–295, 2011.

[77] V. Rajabov, S. Z. Miska, L. Mortimer, M. Yu, M. E. Ozbayoglu, *et al.*, "The effects of back rake and side rake angles on mechanical specific energy of single pdc cutters with selected rocks at varying depth of cuts and confining pressures," IADC/SPE Drilling Conference and Exhibition, 2012.

[78] Z. Cheng, M. Sheng, G. Li, Z. Huang, X. Wu, Z. Zhu, and J. Yang, "Imaging the formation process of cuttings: Characteristics of cuttings and mechanical specific energy in single pdc cutter tests," *Journal of Petroleum Science and Engineering*, vol. 171, pp. 854–862, 2018.

[79] C. Wang, S. Li, and L. Zhang, "Evaluation of rock abrasiveness class based on the wear mechanisms of pdc cutters," *Journal of Petroleum Science and Engineering*, vol. 174, pp. 959–967, 2019.

[80] J. R. A. Chau, *Investigation of the Cutting Process in Sandstones with Blunt PDC Cutters*. Ph. D. Thesis, University of London (Imperial College of Science, Technology and Medicine), London, United Kingdom, April 1992.

[81] C. Lasserre, "Rock friction apparatus: Realisation de tests de coupe sur roches a l'aide d'un outil PDC," tech. rep., Paris, France, 1994.

[82] B. Akbari and S. Miska, "The effects of chamfer and back rake angle on PDC cutters friction," *Journal of Natural Gas Science and Engineering*, vol. 35, pp. 347–353, 2016.

[83] H. Huang, *Discrete Element Modeling of Rock-tool Interaction*. Ph.D Thesis, Faculty of the Graduate School of the University of Minnesota, Minneapolis, Minnesota, U.S.A., December 1999.

[84] P. L. Menezes, "Influence of friction and rake angle on the formation of built-up edge during the rock cutting process," *International Journal of Rock Mechanics and Mining Sciences*, vol. 88, pp. 175 – 182, 2016.

[85] E. Detournay and A. Drescher, "Plastic flow regimes for a tool cutting a cohesive-frictional material," (Swansea, UK), pp. 367–376, Proceedings of the 4th International Symposium on Numerical Models in Geomechanics, A a Balkema, August 1992.

[86] D. A. Glowka, "Use of single-cutter data in the analysis of PDC bit designs: Part 1-development of a PDC cutting force model," *Journal of Petroleum Technology*, vol. 41, no. 08, pp. 797–849, 1989.

[87] W. W. Samiselo, "Rock-tool friction as a cuttability predictor," M.Sc Thesis, Imperial College, London, United Kingdom, 1992.

[88] J. I. Adachi, "Frictional contact in rock cutting with blunt tools," m. Sc Thesis, Civil Engineering, University of Minnesota, 1996.

[89] F. D. Dagrain, "Influence of the cutter geometry in rock cutting with PDC cutters: an experimental approach.," m.Sc Thesis, Department of Civil Engineering, University of Minnesota, 2001.

[90] J. R. A. Chau, *Investigation of the cutting Process in sandstones with blunt PDC cutters*. Ph.D Thesis, University of London, 1992.

[91] I. Rostamsowlat, "Effect of cutting tool properties and depth of cut in rock cutting: an experimental study," *Rock Mechanics and Rock Engineering*, vol. 51, no. 6, pp. 1715–1728, 2018.

[92] T. Lhomme, "Frictional contact at a rock-tool interface: An experimental study," m. Sc Thesis, University of Minnesota, 1999.

[93] F. Dagrain, *Etude des mecanismes de coupe des roches avec couteaux Uses - Approche des mécanismes de frottement sous les couteaux par le concept du troisième corps*. Ph.D Thesis, Faculté Polytechnique de Mons, 2006.

[94] Z. Cheng, G. Li, Z. Huang, M. Sheng, X. Wu, and J. Yang, "Analytical modelling of rock cutting force and failure surface in linear cutting test by single pdc cutter," *Journal of Petroleum Science and Engineering*, vol. 177, pp. 306–316, 2019.

[95] I. Rostamsowlat and B. Evans, "Determination of internal friction angle of rocks using scratch test with a blunt PDC cutter," *Rock Mechanics and Rock Engineering*, vol. Submitted, 2022.

[96] M. Yahiaoui, J.-Y. Paris, K. Delbé, J. Denape, L. Gerbaud, and A. Dourfaye, "Independent analyses of cutting and friction forces applied on a single polycrystalline diamond compact cutter," *International Journal of Rock Mechanics and Mining Sciences*, vol. 85, pp. 20–26, 2016.

[97] L. Hibbs Jr and R. Wentorf Jr, "Borazon and diamond compact tools," *High Temp. High Pressures*, vol. 6, no. 4, pp. 409–413, 1974.

[98] M. Yahiaoui, L. Gerbaud, J.-Y. Paris, J. Denape, and A. Dourfaye, "A study on PDC drill bits quality," *Wear*, vol. 298-299, pp. 32 – 41, 2013.

[99] M. Yahiaoui, J.-Y. Paris, K. Delbé, J. Denape, L. Gerbaud, C. Colin, O. Ther, and A. Dourfaye, "Quality and wear behavior of graded polycrystalline diamond compact cutters," *International Journal of Refractory Metals and Hard Materials*, vol. 56, pp. 87–95, 2016.

[100] J. Sarout, L. Esteban, C. Delle Piane, B. Maney, and D. N. Dewhurst, "Elastic anisotropy of opalinus clay under variable saturation and triaxial stress," *Geophysical Journal International*, vol. 198, no. 3, pp. 1662–1682, 2014.

[101] J. Dautriat, J. Sarout, C. David, D. Bertauld, and R. Macault, "Remote monitoring of the mechanical instability induced by fluid substitution and water weakening in the laboratory," *Physics of the Earth and Planetary Interiors*, vol. 261, pp. 69–87, 2016.

[102] J. Sarout, Y. Le Gonidec, A. Ougier-Simonin, A. Schubnel, Y. Guéguen, and D. Dewhurst, "Laboratory micro-seismic signature of shear faulting and fault slip in shale," *Physics of the Earth and Planetary Interiors*, vol. 264, pp. 47–62, 2017.

[103] H. Velcin, J. Dautriat, J. Sarout, L. Esteban, and B. Godel, "Experimental reactivation of shear-fractured berea and boise sandstones by brine or liquid co2 injection at depth," *Journal of Geophysical Research: Solid Earth*, vol. 125, no. 2, p. e2019JB018281, 2020.

[104] R. P. Borgaonkar, "Influences of cutter wear flat inclination and surface roughness on friction coefficient and contact stress - an experimental approach," M. Sc Thesis, School of Mechanical Engineering, University of Western Australia, 2008.

[105] C. Peña, "An experimental study of the fragmentation process in rock cutting," Master of Science Thesis, Faculty of the Graduate School of the University of Minnesota, Minneapolis, Minnesota, U.S.A., December 2010.

[106] M. Goossens, F. Mittelbach, and A. Samarin, *The LaTeX Companion*. Reading, Massachusetts: Addison-Wesley, 1994.

[107] D. Knuth, *The TeXbook*. Reading, Massachusetts: Addison-Wesley, 1986.

[108] L. Lamport, *LaTeX — A Document Preparation System*. Reading, Massachusetts: Addison-Wesley, second ed., 1994.

[109] H. Munoz, A. Taheri, and E. Chanda, "Rock drilling performance evaluation by an energy dissipation based rock brittleness index," *Rock Mechanics and Rock Engineering*, vol. 49, no. 8, pp. 3343–3355, 2016.

[110] X. He, C. Xu, K. Peng, and G. Huang, "On the critical failure mode transition depth for rock cutting with different back rake angles," *Tunnelling and Underground Space Technology*, vol. 63, pp. 95–105, 2017.

[111] X. B. Li, D. A. Summers, G. Rupert, and P. Santi, "Experimental investigation on the breakage of hard rock by the PDC cutters with combined action modes," *Tunnelling and Underground Space Technology*, vol. 16, no. 2, pp. 107–114, 2001.

[112] D. Che and K. Ehmann, "Experimental study of force responses in polycrystalline diamond face turning of rock," *International Journal of Rock Mechanics and Mining Sciences*, vol. 72, pp. 80 – 91, 2014.

[113] K. Miyazaki, T. Ohno, H. Karasawa, and H. Imaizumi, "Performance of polycrystalline diamond compact bit based on laboratory tests assuming geothermal well drilling," *Geothermics*, vol. 80, pp. 185–194, 2019.

APPENDICES

Appendix A

Drawings of the rock cutting machine

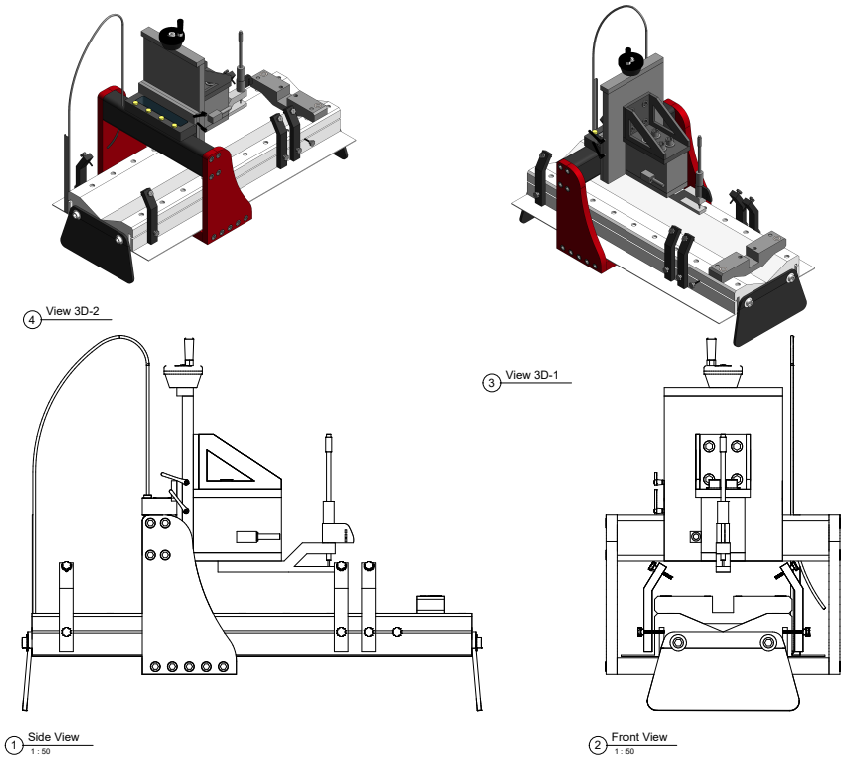


Figure A.1: Schematics of rock scratching device.

Appendix B

Drawing of the cutter holder to change the inclination angle

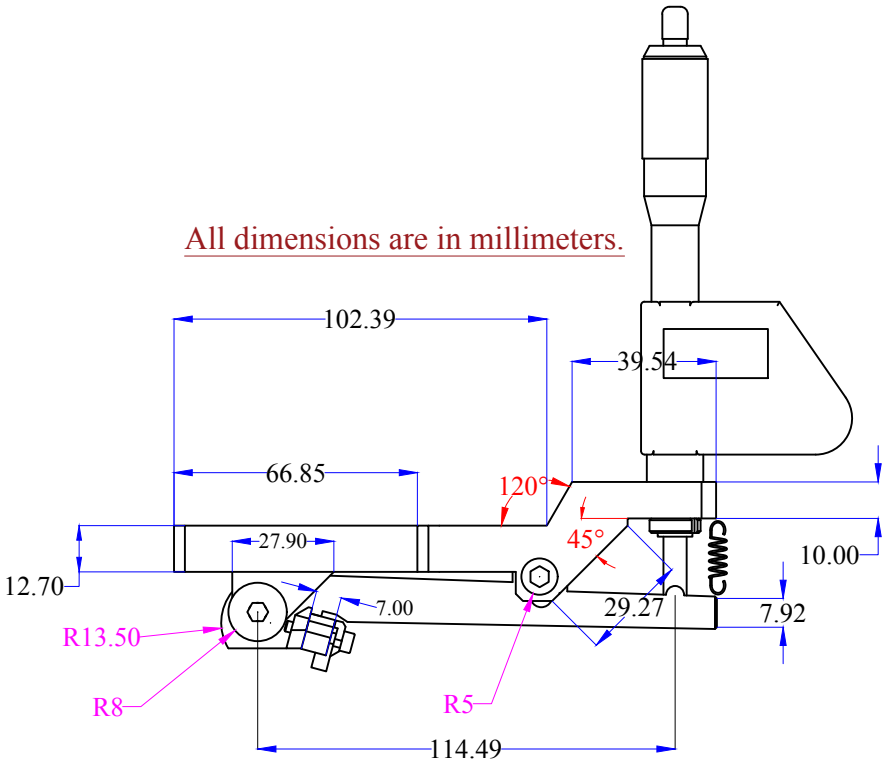


Figure B.1: Drawing of the cutter holder used to change the inclination angle β (or the back rake angle θ).